

Review

# THz Pulsed Imaging in Biomedical Applications

Annalisa D'Arco <sup>1,\*</sup>, Marta Di Fabrizio <sup>2</sup>, Valerio Dolci <sup>1,2,3</sup>, Massimo Petrarca <sup>1,3</sup> and Stefano Lupi <sup>2,4</sup>

<sup>1</sup> INFN-Section of Rome 'La Sapienza', P.le Aldo Moro 2, 00185 Rome, Italy; valerio.dolci@roma1.infn.it (V.D.); massimo.petrarca@uniroma1.it (M.P.)

<sup>2</sup> Physics Department, University of Rome 'La Sapienza', Piazzale Aldo Moro 5, 00185 Rome, Italy; martadifabrizio@gmail.com (M.D.F.); stefano.lupi@roma1.infn.it (S.L.)

<sup>3</sup> SBAI-Department of Basic and Applied Sciences for Engineering, Physics, University of Rome 'La Sapienza', Via Scarpa 16, 00161 Rome, Italy

<sup>4</sup> INFN-LNF Via E. Fermi 40, 00044 Frascati, Italy

\* Correspondence: annalisa.darco@roma1.infn.it

Received: 13 December 2019; Accepted: 24 March 2020; Published: 1 April 2020



**Abstract:** Recent advances in technology have allowed the production and the coherent detection of sub-ps pulses of terahertz (THz) radiation. Therefore, the potentialities of this technique have been readily recognized for THz spectroscopy and imaging in biomedicine. In particular, THz pulsed imaging (TPI) has rapidly increased its applications in the last decade. In this paper, we present a short review of TPI, discussing its basic principles and performances, and its state-of-the-art applications on biomedical systems.

**Keywords:** terahertz spectroscopy; terahertz time-domain spectroscopy; terahertz pulsed imaging; near-field imaging; biomedical imaging; cancer diagnosis; endoscopy

## 1. Introduction

The increasing request for diagnosis techniques in the biomedical area, able to provide morphological, chemical and/or functional information for early, noninvasive and label-free detection, has led to hard cooperation in different scientific fields. Driven by technological advances, a plethora of new modern diagnostics systems is investigated and validated, as complementary biomedical techniques to the conventional ones, covering various scales, from macromolecules to tissues/organs. Among them, worthy of special mention are: infrared (IR) imaging [1,2], scanning near-field microscopy [3,4], photoacoustic microscopy [5], ultrasonic imaging [6], optical coherence tomography [7,8], digital holography microscopy [9–11], Raman scattering microscopy [12], Coherent Raman Scattering (CRS) spectroscopic imaging [13–23], two-photon fluorescence (TPF) [19,24] and second-harmonic generation (SHG) imaging [25–27], and super-resolved imaging techniques [28–31].

Many efforts were done in THz technology, improving THz sources and detectors' responses [32–38], and ensuring devices' flexibility and portability, in recent decades. This has stimulated a wide diffusion of THz systems for spectroscopic and imaging purposes, applicable in various science fields like biology and medicine [39–44], gas sensing [45], chemical analysis [46,47], new materials characterization in low-frequency range and non-destructive evaluation of composite materials and constructions [48,49], astronomy [50], microelectronics and security [51–53], agri-food industry [54], art conservation [55], etc. Thus, alongside these techniques, TPI has been developed and applied in the field of biomedicine.

THz radiation has a variety of properties that make this spectral region a viable spectroscopic imaging technique. First of all, (i) THz radiation has low photon energy (4 meV at 1 THz), coinciding with the energy levels related to rotational and vibrational molecule modes and intermolecular vibrations,

such as hydrogen bonds. These low-frequency motions allow the identification of biomolecules, characterizing their spectral features in THz region [56,57]. (ii) In addition, the low photon energy is insufficient to cause atoms ionization. (iii) For this reason, it is suitable and attractive for noninvasive biomedical imaging, has a great potentiality and could be applied in vivo real-time studies without causing biological ionizing damage, unlike X- and  $\gamma$ -rays [42,43]. Whereas extremely low frequency electromagnetic fields have been long studied in relation to their possible human health effects, the biological effects of radiofrequency and THz signals have come under scrutiny. In particular, the effects of THz radiation are of interest because of the expanding THz technologies in biomedical applications. The prevailing view is that THz radiation, if thermal effects are not considered, does not damage directly the DNA, but it could act as a co-inductor for non-thermal effects [58]. Recent studies show evidence of potential thermal and non-thermal effects induced by exposure to THz radiation [59,60]. The biological response to this stimulus is due to different parameters: the physical settings of the THz radiation (frequency, mean and peak power, radiation intensity, continuous or pulsed radiation, the degree of coherence, etc.); the physical and biological properties of the irradiated biological object (refractive index, absorption features, type of cells, tissues, organs) and the design of the exposure [60]. (iv) In addition, THz radiation is very sensitive to polar molecules, like water. (v) That is why the strong absorption, due to water molecules ( $220\text{ cm}^{-1}$  for pure water at 1 THz and room temperature) [43], limits THz penetrability into the fresh tissues from tens to hundreds microns [42] and the capability of diagnostic only for superficial layers in vivo. (vi) The high sensitivity of water content can be used like an endogenous marker for the differentiation between fresh healthy and pathological tissues [42,43]. (vii) In particular, the time-domain spectroscopy (TDS) and imaging are insensitive to the thermal background and show high signal-to-noise ratio (SNR) [61]. (viii) TPI coherent detection ensures the record of temporal profile of the THz electric field; so, both the THz amplitude and phase can be estimated. From these, the broadband absorption coefficient and refractive index of a medium are determined, without using Kramers–Kronig relations [57,61]. The absorption is generally due to the chemical constituents of the material; thus, its spectral signatures are measured, providing useful information. As consequence, TPI has the potential to realize images with both morphological and functional information, in this frequency range. For all these reasons, THz radiation is considered very important and deserves special attention.

In this review, we introduce TPI, discussing its basic principles and performances, and the state-of-the-art applications on biomedical systems.

The review is organized as follows: in the first section, we outline the main features of pulsed THz systems and their key role in THz imaging setups, showing the equipment needed and some application ideas. Later, in the following section, after summarizing the main properties of the THz contrast image, we also focus on TPI challenges and relevant results achieved in the biomedical field.

## 2. THz Pulsed System/Imaging

Over the past two decades, THz generation and detection technology has considerably advanced, and several devices are commercially available now [33–37,62,63]. Their development has led to various spectroscopic and imaging techniques in the THz spectral window. According to THz sources used, the systems are divided into two general categories: the continuous wave (CW) systems, which produce a single or several discrete frequencies, and pulsed systems, characterized by a broadband frequency output, introduced for the first time as potential imaging tool in 1995 by Hu and Nuss [64]. All of them feature a large variety of properties, as well as, frequencies, power and sensitivity. In this paragraph, we briefly discuss the most common TPI systems that are the aim of our review, with a strong emphasis on THz pulsed sources and detectors.

### 2.1. Generation and Detection of THz Pulsed Radiation

In TPI systems, a broadband frequency emission, from tens or hundreds of GHz up to several THz, is obtained. Currently, various modalities can be listed for generating and detecting pulsed

THz radiation [65,66]: biased photoconductive antennas (PCAs) [67–69], optical rectification (OR) in nonlinear optical (NLO) crystals [70–72], THz production by plasma in air [73–75] and carrier tunneling in coupled double quantum well structures [76–78]. They exhibit different physical properties concerning powers, used materials, covered spectral range, SNR and dynamic range (DR). Among them, the most established approaches, based on PCAs and on OR, require pumping made by expensive infrared femtosecond lasers, often emitting in the near-infrared (NIR) region. For the first mentioned, a pulsed laser beam illuminates PCA gap, made of high resistive semiconductor thin film with two electrical contact pads. Thus, in the presence of the applied bias voltage and laser beam, photocurrent is generated and the static bias field accelerates the free carriers producing broadband frequency THz waves into the free space.

OR ensures the THz broadband generation through NLO centrosymmetric crystals [70–72], extended from 0.1 THz and beyond 40 THz [57,79,80], such as organic NLO crystals. 4-N,N-dimethylamino-4'-N'-methyl-stilbazolium 2,4,6-trimethylbenzenesulfonate (DSTMS) [81–84] and 4-N,N-dimethylamino-4'-N'-methyl-stilbazolium tosylate (DAST) show efficient generation from 0.3 to >16 THz in the phase-matching condition between 720 nm and 1650 nm. The NLO materials need to have high second-order NLO susceptibility, high transparency at both pump and THz frequency, and high optical damage threshold, in order to satisfy the phase-matching condition between the fundamental optical pump and generated THz waves [85,86]. When intense NIR laser beams propagate through some crystals, second order nonlinear effects occur, developing a DC or low frequency polarization [38]. This leads to the radiation of an electromagnetic single-cycle pulse with a wide frequency spectrum, ranging roughly from zero frequency to some maximum value [38].

Another way to produce THz radiation is by charges acceleration. As consequence, the charges radiate electromagnetic waves, that under particular conditions, lie in the THz region of the electromagnetic spectrum. The processes can be done either within semiconductors, in vacuum or in air [87–90]: via electrons acceleration by the intense laser pulse [87,88], by an applied bias voltage across an air gap, similarly to PCA, or by nonlinear four-wave mixing of the fundamental and the second harmonic frequencies of the laser beam, in air or in various gases [89,90].

Besides OR, photoconduction or photocurrent, surge is another primary mechanism for THz generation from semiconductor materials [57,59]. When semiconductor quantum wells (QWs) are under a bias, the mechanism for THz generation is attributed to the creation of polarized electron–hole pairs [91–93].

In its turn, two schemes are ideal to THz pulse detection, based on incoherent and coherent techniques. In terms of incoherent techniques, power-to-signal transducers, suitable for incoming energy measurements, are used. For coherent ones instead, the detectors give information concerning the power, frequency spectral range and phase of the incoming electrical signals [57]. Among THz incoherent detectors commercially available, we can mention bolometers [94]; Golay-cells, providing stable performances and high sensitivity; and pyroelectric detectors [95] and thermopiles with low sensitivity. Commercial bolometers, resistive temperature sensors, widely used in THz spectral region, are cryogenic ones. The cooling of the devices ensures high sensitivity, with noise equivalent powers (NEPs) ranging from  $10^{-12}$  W/Hz<sup>1/2</sup> to  $10^{-14}$  W/Hz<sup>1/2</sup>. Golay-cell detectors [96] measure the thermal energy of THz propagating through a window [61]. Their spectral performances are strongly dependent on the material used for the window. In the case of diamond and crystal quartz windows, the spectral range covers from millimeters-wave to visible frequencies [61], while for HDPE (High-Density Polyethylene) window the spectral range is upper bounded at ~20 THz. Power DR can vary from hundreds nW up to 1 mW, with power DR from hundreds nW up to 1 mW. These devices can reach excellent NEPs at room temperature—around  $\sim 10^{-10}$  W/Hz<sup>1/2</sup> [61]. Instead, pyroelectric devices show lower sensitivity (NEPs  $\sim 10^{-9}$ – $10^{-10}$  W/Hz<sup>1/2</sup>) compared to bolometers and Golay performances. Table 1 summarizes some performances of the most used incoherent THz detectors.

**Table 1.** Main incoherent detectors suitable for THz spectral range with their performances: noise equivalent powers NEPs, THz coverage and detector bandwidth, linked to the detector response time (the higher the bandwidth, the faster the response time). Bolometer, Golay cell and Pyroelectric are pure incoherent detectors, while Schottky diode is used both for coherent and incoherent measurements.

Detector	NEP (W/ Hz <sup>1/2</sup> )	THz Coverage (THz)	Bandwidth (Hz)
Cryogenic Bolometer	10 <sup>-14</sup> –10 <sup>-12</sup>	0.1–30	10 <sup>2</sup> –10 <sup>3</sup>
Golay cell	10 <sup>-10</sup>	0.01–20 <sup>1</sup> 0.01–700 <sup>2</sup>	10–10 <sup>2</sup>
Pyroelectric	10 <sup>-10</sup> –10 <sup>-9</sup>	0.1–10	10–10 <sup>8</sup>
Schottky diode	10 <sup>-14</sup> –10 <sup>-11</sup>	0.1–2	10 <sup>2</sup> –10 <sup>6</sup>

<sup>1</sup> High-Density Polyethylene (HDPE) window; <sup>2</sup> Diamond window.

THz cameras were the object of intense research activities in recent years. Actually, various THz cameras, based either on cooled and uncooled bolometers or semiconductor devices, are commercially available. Among the THz thermal cameras, the Golay cells are slow detectors and are difficult to integrate into array detectors. Consequently, the imaging scheme for them is a single-pixel detector [97]. The pyroelectric cameras, like the Pyrocam series sold by Ophir Optics, can operate with pulsed and CW sources, as well as thermopile cameras [98,99]. Generally, they are widely commercially available, and their low sensitivity makes them less attractive for THz imaging. The microbolometric cameras are arrays of bolometers; because of the relatively higher sensitivity they are considered the prime candidates for THz imaging. When cooled at cryogenic temperatures, they can achieve NEPs around 10<sup>-16</sup> W/Hz<sup>1/2</sup>. With proper design modifications, microbolometric cameras at room temperature also achieve high enough sensitivity.

Many such imaging techniques cannot be realized with existing THz cameras, but require a coherent detection scheme. Among commercial coherent or heterodyne detectors, largely used, we mention: Schottky diodes [100,101], PCAs and NLO crystals or via electro-optical (EO) effect in nonlinear crystals [70–72]. Schottky diodes [100,101] show limited spectral bandwidth around 1–2 THz and NEPs up to 10<sup>-14</sup> W/Hz<sup>1/2</sup>, and actually they are the object of research. PCAs (frequency range limited <10 THz and NEPs around 10–12 W/Hz<sup>1/2</sup>) can detect a THz electric field profile with a coherent detection scheme. The probe beam, derived from the same laser used to generate the THz radiation, irradiates receiver PCA, which has no external bias voltage. The laser pulses gate the detector acting as a photocurrent switch by generating charge carriers. The incoming THz radiation, on the receiver, induces the bias voltage, thus the photocarriers are accelerated [67,69]. The transient current is measured by a low-current amplifier and a lock-in technique, that are referenced against a modulation placed on the PCA emitter bias voltage.

In EO rectification NLO crystals, instead, the THz field induces birefringence in them; at a given instant, the polarization state of the probe laser pulse changes proportionally to the THz field amplitude [25,102]. Then, a balanced photodiode is used for measuring these changes in birefringence, reconstructing the THz pulse. In recent years, great interest in THz sensors and cameras is focused on the development of devices with high sensitivity, which operate at room temperature and fast operation speed [103], such as optoelectronic sensors and detectors [104–107].

## 2.2. TPI Equipment

The switch from the spectroscopy system to the imaging one is based on the possibility to collect spectroscopic information on large sample areas. For this purpose, the point-by-point signal collection requires a mechanism for scanning: moving the beam or the sample holder. The first case is realized with a beam motion or oscillating objective; using for example, galvo-mirrors and/or piezoelectric rotator or stages. In the second case, the lateral translation of the specimen stage is combined with a stationary illumination; for this purpose, a 3D linear translation stage is used, allowing sample holder motion along the THz beam (1D motion) and perpendicularly to it (2D motion).

The acquisition speed is one of the most critical challenges when using THz radiation for biomedical imaging, and it requires more attention for the implementation of clinical devices. The imaging speed depends on the specific image scheme chosen: using a point source and detector, the acquisition is slow, due to the point-by-point sample scanning. Although, the two-dimensional galvo-scanner, combined with a fast detector or sophisticated signal processing techniques [108–110], improves the scanning speed and the acquisition on a large field of view.

The object surface is illuminated by the THz beam, and it is sampled on a discrete grid, scanned in continuous or pixel-by-pixel raster modes. The information collected in each pixel is digitalized, transferred to PC from a data acquisition card (DAQ) and quantized in a finite number of bits for pre- and post-image processing.

### 2.2.1. TPI Far-Field Systems

A typical pulsed THz wave generation and detection system is a pump-probe setup. It can be considered as an extended THz time-domain spectroscopy (THz-TDS) method. The basic idea of THz-TDS and TPI systems is illustrated in Figure 1a.

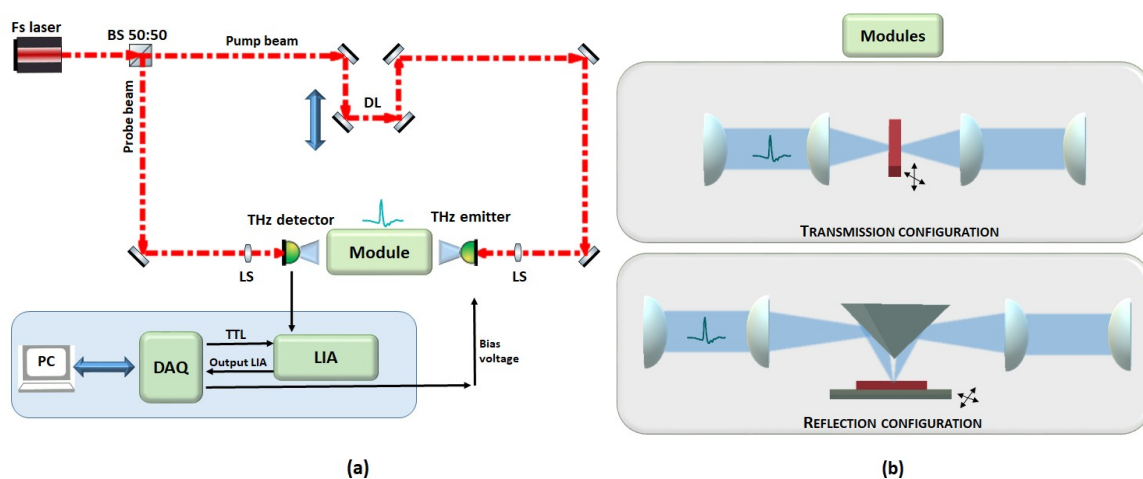


**Figure 1.** This is an example of TPI system switched by PCAs. (a) The schematic layout of common TPI system based on photoconductive switches. Here, Fs laser stands for femtosecond laser, BS for beamsplitter, DL is the delay line, LS are lenses, LIA, DAQ and PC stand for lock-in amplifier, data acquisition card and desktop computer, respectively. (b) The schematic layout of two potential sample orientation: transmission and reflection modes. The standard transmission imaging configuration involves the specimen placed between THz low-absorption material plates or standing in free space. The generated THz signal travels at a normal incidence to the sample surface and the transmitted one is received on the other side of the sample. Instead, for reflection mode, the THz signal illuminates one sample surface and it is reflected by the same surface.

TPI system, shown in Figure 1a, is powered by a femtosecond laser. A beamsplitter splits the initial laser beam into two parts: the pump and the probe beams. The pump beam is modulated via an optical or mechanical chopper or by modulating the THz emitter bias voltage, and then is focused on the THz emitter. The generated THz radiation is then collimated and focused onto a target sample. When a THz pulse illuminates a target, a train of THz pulses will be reflected from the various interfaces or transmitted. The transmitted (Figure 1b) and/or the reflected (Figure 1b) electric fields are, then, recollimated and refocused onto THz detector using THz transparent lenses or parabolic mirrors. The electrical signal is filtered and detected by lock-in amplifier detection. The analog output of the lock-in amplifier is collected and digitalized by a dedicated DAQ. A delay line is used in order to temporally sample the THz electric field. Thus, for each individual pulse in the detected signal, the amplitude and phase are different and are measured too.

If the pump and probe optical paths are equal, the THz electric field is measured at one fixed instant in time. In order to sample the whole THz pulse, a delay line is introduced in the optical scheme, to delay pump and probe beams. Generally, this can be performed using a mechanical translation stage, that moves at fixed steps; but rapid-scanning delay lines can also be used to speed the acquisition [111,112].

For example, we reported our home-made TPI system based on THz-TDS (see Figure 2a). It was implemented in transmission configuration.

It generates broadband THz radiation (0.1–3.5 THz) via photoconductive switches, used both for THz emission and detection. We use a mode-locked ultrafast laser (FemtoFiber NIRpro, Toptica), at 780 nm with a 100 fs temporal pulse width and a repetition rate of 80 MHz to illuminate twin G10620-11 Hamamatsu PCAs. The femtosecond laser is split into two beams by a 50:50 beamsplitter—each beam has 15 mW average power. Dielectric mirrors deflect the beams towards emitter and detector PCAs. TPX lenses are used to collimate and focalize THz radiation. The object is aligned in the focus of the THz beam, perpendicularly to the propagating THz radiation. The point-by-point spectral signal collection is obtained by scanning a large area of the object with 3D axes stage (Thorlabs). After transmission through the sample, THz pulses are collimated and refocused on the THz-detector PCA by TPX lenses. Simultaneously, the probe beam is used to gate the THz-detector PCA. The THz electric field as a function of time is measured with a delay line [112]. The output signal from the THz-detector, extracted by a lock-in amplifier (Stanford, SR830), is transferred to a National Instrument acquisition card (NI 6361-BNC connector) allowing the data collection. Our system exhibits performances comparable with the commercial systems, and being a home-made spectrometer, it can switch on the other two spectroscopic configurations using metallic flip mirrors, inserted in the THz collimated region. We can select between THz–TDS reflection spectroscopy and attenuated total reflection (ATR) spectroscopy, see Figure 2a.

In Figure 2b, the temporal electric field profile, in free-space, as a function of time, is reported with relative power spectrum, for the scheme in transmission.

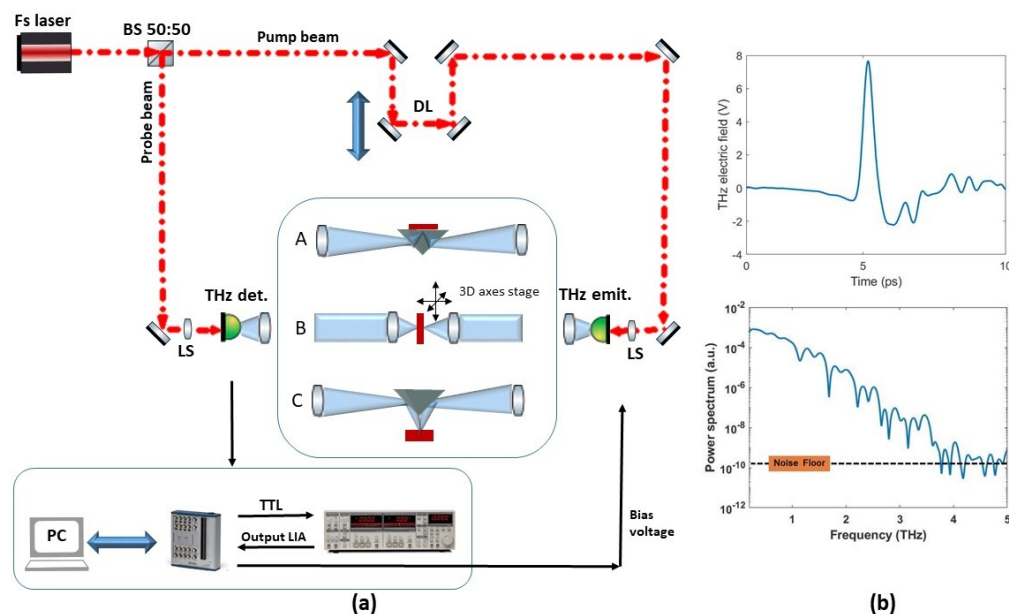


**Figure 2.** (a) Schematic layout of our TPI system. In the scheme, Fs laser stands for femtosecond laser, BS for beamsplitter, DL for delay line, LS is referred to lenses, THz det. and THz emit. are THz detector and THz emitter respectively. With two metal flip mirrors, introduced in the collimated THz beam region, one can select the scheme for THz spectroscopic imaging in transmission (B) or reflection (C) or ATR (A) spectroscopy. (b) The temporal electric field profile, in free-space, as a function of time, is reported with relative power spectrum.

### 2.2.2. TPI Near-Field Systems

The major limitation of THz far-field imaging systems is due to the problem of the diffraction-limited spatial resolution central to THz wavelengths, compared, for example, to visible radiation [113,114]. The optical resolution  $R$  in the object plane is generally defined by the Rayleigh criterion [115–118], described as:

$$R = \frac{0.61 \cdot \lambda}{NA} \approx \frac{\lambda}{2NA}$$

at the wavelength  $\lambda$  and numerical aperture  $NA$ . The minimal resolvable feature corresponds to the minimum size, in the object plane, of the smallest object that the optical system can resolve: as the resolution is directly proportional to the wavelength and inversely proportional to the numerical aperture of the optical components, at 1 THz the resolution turns out to be around 0.5 mm [113]. In fact, 1 THz corresponds to 0.3 mm and one must consider the loss of resolution caused mostly by lenses on the beam path. For this reason, effective and wide spreading of THz images in biomedical research and diagnostics is difficult. The wavelength-limited resolution is caused by diffraction of propagating waves, so this problem can be overcome by collecting THz pulses in near-field (NF), namely at a distance with the sample comparable to the wavelength. In this way, evanescent waves, that propagate only very close to the sample and then rapidly decay, can be detected. That is the reason why THz detector must be placed in proximity of the sample. Several techniques have been explored to enable sub-wavelength THz imaging [37,114,119,120]. With this purpose, detectors and sources of different shapes can be used; in particular, Hunsche et al. [121] proposed and demonstrated, for the first time, a method deriving from the confocal microscopy. It uses pinholes that act as spatial filter, reducing the THz beam size to sub-wavelength dimensions and blocking outside the cone of light. This results in increased lateral and depth resolutions [122,123]. However, the aperture introduces an immense loss of THz light intensity at deep sub-wavelength resolutions ( $<\lambda/10$ ) [124], caused by the low frequency cut-off [125] and optical coupling loss. Following, it is possible to place a small detector or emitter directly behind the aperture [126–128]. The approaches without apertures, instead, are better set to achieve deep sub-wavelength resolutions, because the low-frequency cut-off is avoided. The sharp metallic tips for local field enhancement, tip apex, small detectors and/or sources elements with sub-wavelength dimensions are placed in proximity of the sample surface or in direct-contact. In this way, high resolutions are achieved (even  $\lambda/100$ ), with the only limitations imposed by the tip diameter [129]. This means that NF resolution is not limited by diffraction so that, in this way it becomes independent of the wavelength.

The direct-contact approach, instead, is generally employed with EO sampling using THz-TDS. The sample could be then in contact with the detection crystal, leading to a direct measurement of the THz electric field in NF region. In [130], the deposition of various metal structures onto a gallium phosphite (GaP) crystal can improve the resolution by imaging at 20  $\mu\text{m}$ .

### 3. Basics of THz Imaging

TPI can be viewed as an extension of the THz-TDS method. The classic way to obtain THz imaging from THz-TDS is illustrated above. In order to image the objects, a 2D point-by-point raster scanning of them, combined with a coherent detection, is performed; and the individual temporal profiles are recorded for each point-pixel. The raw one-dimensional time or extracted frequency data are converted into physical values [57,61,64,131,132]. The normalization is chosen to enhance the image contrast, and it can be summarized in the diagram (Figure 3).

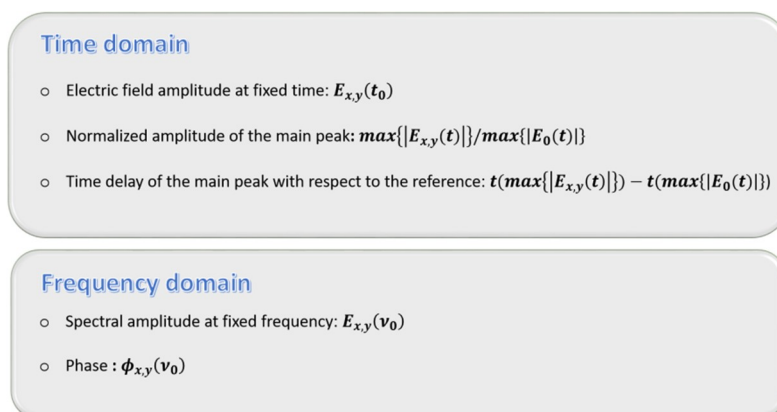


**Figure 3.** Schematic summary concerning the image contrast in THz-TDS imaging.

In time domain, when there is interaction with the sample, the THz pulse can be attenuated, delayed or broadened, compared to the reference without the sample, generally measured in air. The electric field amplitude, at a fixed time, represents a contrast modality to normalize the image. In addition, the normalized amplitude of the main peak, as the ratio between maxima of the sample and reference electric fields, provides image information regarding the absorption, reflection or scattering losses in the object. Finally, the knowledge of time delay of the main peak with respect to the reference allows mapping the optical path changes, providing material/thickness contrast [133]. For example, the time-of-flight (TOF) technique permits to estimate the depth information about target internal dielectric profiles. A THz pulse is launched to the sample and the reflected echo is measured in amplitude or/and phase. The TOF information of the echo pulse indicates the presence of the boundaries, or inner structures along the THz propagation path, which extracts the one-dimensional depth profile. Thus, by performing a 2D scan, a 3D image of the object can be visualized, viewing into a layered structure or inside the optically opaque materials. 3D imaging potentiality is suitable for the implementation of various imaging techniques, largely used in biomedical contexts. Applying the Fourier transform on the temporal electric pulse, one gets the amplitude and phase of the spectrum. The first gives a general indication of the losses; the second one is related to the refractive index. Fixing the frequency, one can visualize the object in the frequency domain, the amplitude and the phase images [134]. This offers more contrast, because of the sufficiently different refractive indexes of the materials than the losses, which provide a meaningful contrast.

Summarizing, the THz-TDS measurements allow the extraction of both amplitude and phase of THz waveform. The complex refractive index and absorption coefficient can be obtained using the Fresnel coefficients [135,136], and from them the complex permittivity [137,138]. The knowledge of sample spectral behavior ensures to extract information concerning its morphological structure and the optical properties: the variation of refractive indexes could differentiate tissues, and could be related to the pathological status. Moreover, many materials are relatively transparent to THz radiation, and are used in the development of 3D THz imaging modalities that constitute an active research field [107,139]. Tomographic slices are employed for object/tissue 2D or 3D reconstructions, in order to obtain their internal properties and features [111]. The method tried a natural extension for the object rotation towards THz computer tomography (CT) [140,141]. In addition to THz CT, there are several other tomographic techniques based on THz radiation, including THz interaction tomography, THz tomosynthesis, time-of-flight pulsed imaging and 3D THz holography [139].

#### 4. THz Pulsed Imaging: Uses, Advantages and Challenges for Biomedical Applications

As briefly discussed in the introduction and in the previous paragraph, the unique spectral features of THz radiation make this technology particularly interesting in the biomedical field—for ex vivo and in vivo experiments and/or analyses. During the past decades, systematic spectroscopic

investigations carried out in the THz frequency region on biological targets, as biomacromolecule, cells and tissues, demonstrated differences in their optical properties. In the last five years only, the rate of imaging experiments in the THz domain is increasing.

An unavoidable issue, when talking about THz imaging, is water: THz is particularly sensitive to water content, exhibiting a strong absorption [142] and consequently limiting THz penetration depth.

In fact, the strong absorption of water limits the penetration depth in fresh tissues between tens and hundreds of microns. For example, into the human skin THz waves can penetrate only a few hundred microns [143]. In vivo clinical measurements, it limits the probing on superficial layers of the target and the reflection mode becomes the suitable choice [144,145]. The limitation could be overcome in the case of ex vivo examinations, where histopathological evaluations are required. Researchers overcome these limitations using thin and/or fixed samples and appropriate geometry. The transmitted TPI is performed on thin prepared tissues, suitable for in vitro, and reflected TPI allows the investigation of surface features, reliable in vivo and ex vivo imaging.

However, difficulties in extrapolating measurements on tissue to ex vivo include, for example, saline uptake from the sample storage environment, changes in hydration level during the measurement, temperature- and humidity-dependent and scattering effects. Considering that, the human body contains a large amount of water (~60%) and THz is heavily absorbed by water [142], fresh tissue can vastly alter THz spectroscopy measurements. As fresh tissue dehydrates when left exposed to the air, many contrast features are reduced during the data acquisition. Therefore, for biomedical studies, sample conservation is crucial.

Several research groups have investigated excised and fixed tissues considering numerous approaches; among them are dehydration [146,147], alcohol perfused [36], formalin fixed [148–150], gelatin embedding [151,152], lyophilized [153], freezing [154,155] and fixation in paraffin emulsion and embedding [156].

Formalin fixing, in order to preserve and fix excised tissues, is a common histopathological routine for diagnosis. The formalin reduces the sample variation due to the dehydration process [149,154]—the tissues' water content is replaced by formalin.

In addition, lyophilization could represent an interesting alternative to fresh tissue for THz spectroscopic measurements [153]; its pros are fast and effective water removal, and structural preservation. The problems with handling fresh tissue, such as time variability in the THz bandwidth, dynamic range and sample thickness, are therefore overcome [153]. Several studies proposed the freezing of biological sample, as an alternative technique to increase the penetration depth of THz waves in the tissues, as the absorption coefficient of ice is one order of magnitude lower than the absorption coefficient of water [143]. The discussed technique has a limitation in clinical use; the process of freezing might cause necrosis. Some suggestions are proposed by using a penetration-enhancing agent (PEA) to increase the THz radiation delivery depth. The treatment with PEAs, that are cost-effective and easy-to-find, biocompatible and nontoxic to the human body, could also ensure long preservation time for ex vivo tissues and the application in vivo. Oh et al. [157] used glycerol as PEA, easily absorbed by human skin and tissue and with an absorption coefficient much lower than that of water in the THz spectral region. They treated abdominal mouse skin with glycerol and demonstrated the enhancement of penetration depth with the reconstruction of a metal blade hidden under the tissue by the second pulse reflection of it [157].

Various alternative approaches are suggested. Oleic acid is proposed by Wang et al. [158] for trapping moisture inside thin tissue slices, in transmission acquisition mode. They realized a sandwich configuration, by placing a frozen layer of oleic acid above and below the frozen tissue sample, between tsurpica windows and waited for complete thawing, before starting the measurements at room temperature. Oleic acid is highly transparent to THz radiation and its refractive index matched tsurpica. The oleic acid layers were used to keep up the tissue hydration, showing good performances for 70 min. Fan et al. [151] used gelatin embedding for porcine skin slices reflection measurements. By looking at the THz image data and computing the optical parameters of the gelatin-embedded

sample, they found a successful method to preserve the sample for at least 35 h, both for imaging and spectroscopy purposes.

Since the first demonstration of THz imaging [64], TPI and spectroscopy show their ability to differentiate human tissues [141,159], with clear differences between the tissue properties, in particular regarding absorption coefficients [160]. Fatty tissue consists of mainly hydrocarbon chains, largely nonpolar molecules, thus its absorption coefficient and refractive index are much smaller than the ones of muscle, kidney and/or liver tissues [141].

Concerning the optical characterization at the low frequency region, many spectroscopic works are present in the literature [161–167]. One significant work about the ability in distinguishing and classifying the THz response of different types of tissues is Ref. [131], which is mentioned for the chirped probe pulse technique. It offers a significant improvement concerning the slow acquisition time, and it could have great potential in imaging acquisition.

In addition, the high sensitivity of THz waves to water content in the tissues becomes the key contrast factor in many biomedical applications [168,169]; the water content evaluation allows label-free differentiation for various types of tissues as an endogenous marker, distinguishing between healthy and pathological tissues [152,168], see Figure 4.

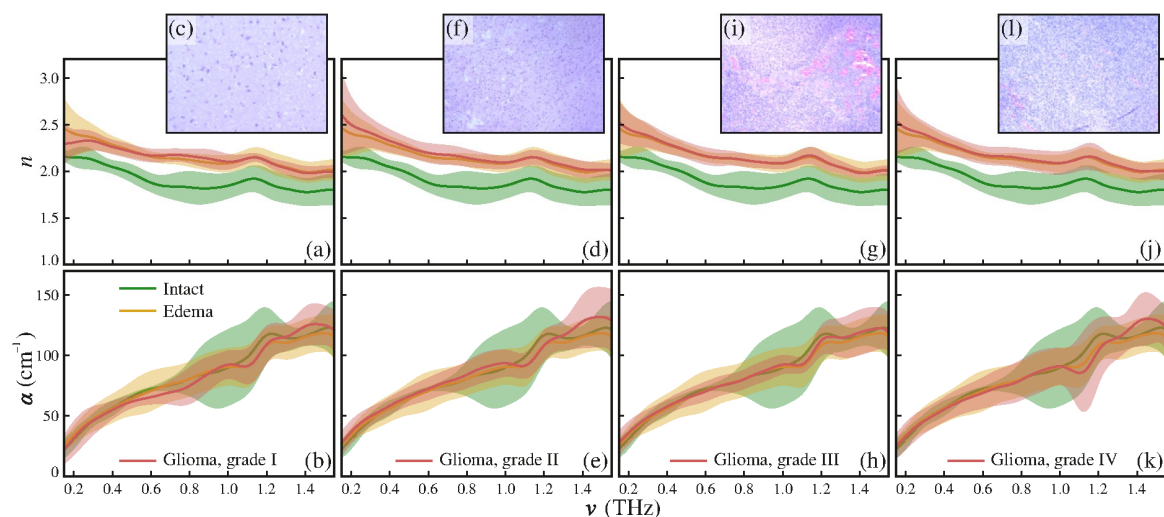


**Figure 4.** Refractive index  $n$  and absorption coefficient  $\alpha$  in THz spectral region, observed by Gavdush et al. [152], and H&E-stained histology of gelatin-embedded ex vivo human tissues: intact tissue, gliomas of grade I to IV, and edema. (a)–(c) grade I; (d)–(f) grade II; (g)–(i) grade III; and (j)–(l) grade IV. The THz optical properties of gliomas are compared with equal data for the intact and edematous tissues, averages within the entire set of brain tissues specimens [152].

In the case of cancer, the contrast between healthy and malign tissue is originated from the structural variation and different water content [170]. In fact, the presence of cancer induces, in many cases, increased blood supply to the affected tissues and a local increase in tissue water content, which suggests water contrast for THz cancer imaging [171]. As a result, it involves a higher refractive index and absorption coefficient [39,169,172]. As proof, Figure 5 shows refractive indexes and absorption coefficients of normal and cancer regions of a fresh rat brain tissue sample, as a function of frequency [39].

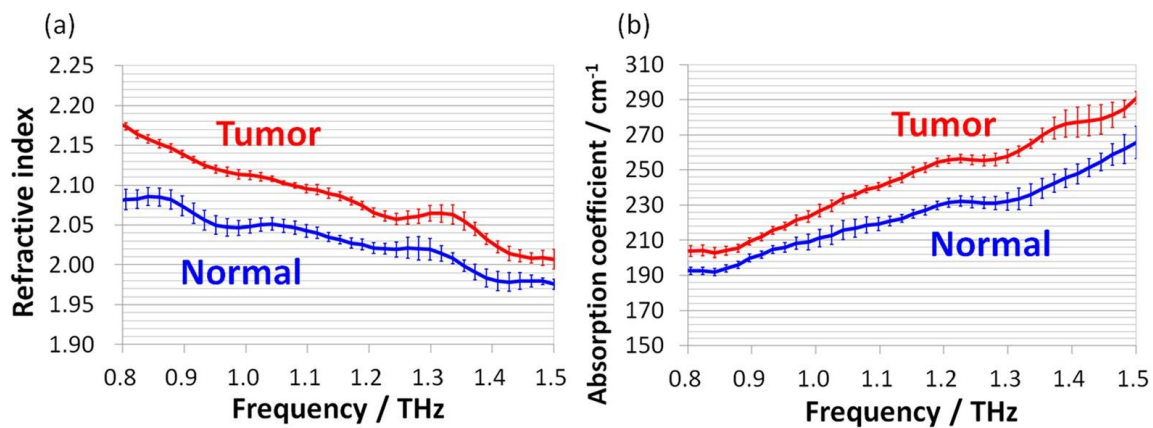


**Figure 5.** Optical characterization of a fresh rat brain tissue sample [39]. (a) Refractive index and (b) Absorption coefficient ( $\text{cm}^{-1}$ ) of normal and tumor regions, from 0.8 to 1.5 THz. Both refractive index and absorption coefficient in the tumor region are higher than in normal tissue due to the higher water content in cancer tissue.

TPI has been successfully applied to liver [164,173,174], colon [165,175,176], intestine [161], brain [39,156,177], skin [178], ovarian [167], oral [154] and breast cancers [132,163,179].

For instance, a particular attention deserves the oral-, gastric- and intestinal- neoplasia, because an early/rapid diagnosis is required. However, it may be quite difficult due to oral-gastric-intestinal apparatus anatomy. Sim et al. [154] used a TPI reflection system in the frequency range of 0.2–1.2 THz to assess oral carcinoma. Seven oral tissues from four patients were analyzed, and then the authors compared the optical, frozen and room temperature THz, histopathological images. They found that THz images at  $-20^\circ\text{C}$  showed better contrast between healthy and cancer regions compared to the room temperature ones ( $20^\circ\text{C}$ ). Additionally, frozen temperature images demonstrated better area correlation than the histopathological images [154]. The recent and detailed review of Danciu et al. [180] takes an overview of diagnostics methods and current available data on THz-based detection for digestive cancers. Some current in vitro and ex vivo progress is highlighted for identifying specific digestive neoplasia [180].

Instead, TPI has revealed the contrast between normal and neoplastic tissue regions [159,181]. One of the first applications on human ex vivo wet tissue involved imaging in excised basal cell carcinoma [182]; the regions had recognition of healthy skin and basal cell carcinoma (BBC), both in vitro [96] or in vivo and ex vivo [183,184].

According to Wallace et al. [184], TPI could differentiate between basal cell carcinoma (BCC) and normal tissue both in vivo and ex vivo, and it is under test whether TPI can facilitate the tumor margins delineation, prior to surgery. The BCC's areas have different THz properties compared to healthy tissue. The general clinical image does not identify the skin cancer distribution with accuracy in depth, under the skin surface. However, THz images, as shown in [184], clearly display the cancer distribution on the skin and also the extent of the neoplasm invasion into the skin, with a depth of  $250\ \mu\text{m}$ .

Comparing ex vivo and in vivo images of the same tumors, similar contrast levels can be found, however tissue deformation and shrinkage after excision leads to an exact match in the contrast pattern. Nevertheless, the contrast level, present in the THz images, was enough to map diseased tissue margins, when compared to histology. Reese et al. [185], using THz pulsed imaging for studying freshly excised colon cancer, have differentiated normal and diseased colon tissues, with a good contrast for their recognition. Moreover, Wahaia et al. [186] measured colon tissue samples both fixed in formalin and embedded in paraffin. In the first case, water is still present, and in the second one, it is eliminated. They still obtained good image contrast between healthy and cancerous regions. As a result, water is not the only factor contributing to the contrast between the two different tissue

areas. Thus, the tumor boundaries in THz images can be recognized, and these are in accordance with the visible images, indicating that the THz imaging technique could be useful for diagnosing cancers. Potentially, this technique could be employed as a complementary label-free technique, allowing surgeons to determine tumor margins in real time.

While different kinds of cancer can be differentiated from healthy tissue according to the high sensitivity of THz radiation to water content, the strong potential of TPI in cancer assessment is not limited to fresh tissues, as it has been efficiently demonstrated for discrimination of pathological and healthy dehydrated tissue as well [132,174,177].

Afterwards, TPI has been used to identify tumor borders on excised breast carcinoma [187]. While THz imaging has proven potential contrast between breast cancer and healthy tissue, both in fresh and formalin-fixed, paraffin-embedded (FFPE) tumors [154,179,188,189], all published works were performed on flat sections of the tumor. The application of THz imaging to a three-dimensional sample can be exploited to produce cross section images by in-depth scanning, without slicing the tumor. Bowman et al. [190], in their work, illustrated the powerful THz pulsed imaging applications to two different carcinoma samples: infiltrating ductal carcinoma and lobular carcinoma, both embedded in paraffin blocks. THz pulsed images showed clear definition of the cancer boundaries in the block. The results were correlated in 3D with histopathology sections sliced throughout the blocks. THz images highlighted the cancer regions only when there were interfaces inside the tissue, thus near to the sample surface. In all the histopathology images, instead, the infiltrating ductal carcinoma and lobular carcinoma were clearly visible, at any section. Furthermore, the THz 3D block images could be sectioned into planar (x-y, x-z, and y-z) images in order to produce in-plane and in-depth tissue images, thus successfully identifying cancer regions, without slicing the tissue. These results demonstrate the effectiveness of THz pulsed imaging for tumor edge identification, when diseased tissue is near the surgical excision.

Reid et al. [176] conducted a study on normal, tumor and dysplastic freshly excised colon samples from 30 patients, using a conventional THz-TDS system, in reflection mode. The study showed a sensitivity of 82% and a specificity of 77% in discriminating between normal and pathological tissues, while a sensitivity of 89% and a specificity of 71% in differentiating normal and dysplastic samples [176]. Another study [191], using diverse intelligent analysis methods (neural networks, decision trees, and support vector machines) re-evaluated the data provided by [191]. This method increased the sensitivity to 90%–100% and the specificity to 86%–90%, improving the overall diagnosis precision.

With the aim of reducing patient re-operation rates and improving the ability of resection margin in breast conserving surgery, Santaolalla et al. [192] applied a multivariate Bayesian classifier to the samples waveform produced by TPI probe system. They can discriminate tumor from benign breast tissue, obtaining a sensitivity of 96% and a specificity of 95%.

Nowadays, in vivo THz detection investigates mostly superficial normal and diseased tissues, close to the epithelial layer (i.e., breast, skin). Observing the significant contrast in THz dielectric permittivity responses of healthy skin, dysplastic and non-dysplastic skin nevi, Zaytsev et al. [193,194] distinguished the precursor of melanoma, with a non-invasive in vivo analysis, proving the efficiency of THz pulsed radiation in the early diagnosis of the melanomas.

To facilitate the use of TPI to scan tumor resection margins intraoperatively, Teraview Ltd. (Cambridge, UK) has proposed and developed a handheld probe system [195]. TPI handheld probe measures tissue sample positioned in histology cassette, in reflection mode. The TPI handheld probe ensures to discriminate benign from malignant breast tissue in an ex vivo setting. The purpose of the THz device is to give valid support for rapid histopathological evaluation of excised tissues in surgery [195].

Despite this, in the last ten years, researchers began to extend THz applications to inner tissues, organs or hollow cavities of the human body. The request is for endoscopic access, achievable using highly bendable waveguides with low transmission loss [196–198]. In 2009, Ji et al. [199] fabricated and developed a miniaturized fiber-coupled THz endoscope apparatus. It emits and collects THz

radiation using an optical fiber linked to a femtosecond laser. The measurement is performed close to the reflective surface of a profound tissue or an organ [199]. The researchers tested the device by looking at THz reflections from mouth, tongue and palm skin tissues and demonstrated that the moisture of internal organs is a significant confounding issue. Some years later, an innovative THz prototype, with single-channel detection based on flexible metal-coated THz waveguides [197,198] and a specific polarization exposure method, was integrated into a commercial optical endoscope and demonstrated its potentiality, successfully differentiating between normal and cancer colonic tissues [175]. This also makes it a suitable tool for investigating the water content and hydration profile of the skin. By using some basic image processing techniques like intensity windowing, histogram manipulation, edge detection and region growing [200–202], the discrimination of healthy and cancer regions by THz images can be considerably improved.

The same group also developed THz otoscope that enables the detection of otitis media [203], a disease that causes fluid and purulence in the posterior part of the tympanic membrane within the middle ear. The THz otoscope is able to measure the change in water content on the tympanic membrane; therefore, it is applicable as a medical device for otitis media diagnosis [203].

In [204] and in Figure 6, an imaging device was proposed as a potential tool for the detection of deterioration in the feet of diabetic patients. Assuming that dehydration of the feet skin of diabetics, owing to peripheral vascular disease, is a central element of their deterioration process, they take advantage of THz pulsed imaging in order to obtain a promising diagnostic tool. The results are encouraging and provide key elements that will allow the design of a clinical trial in the future.

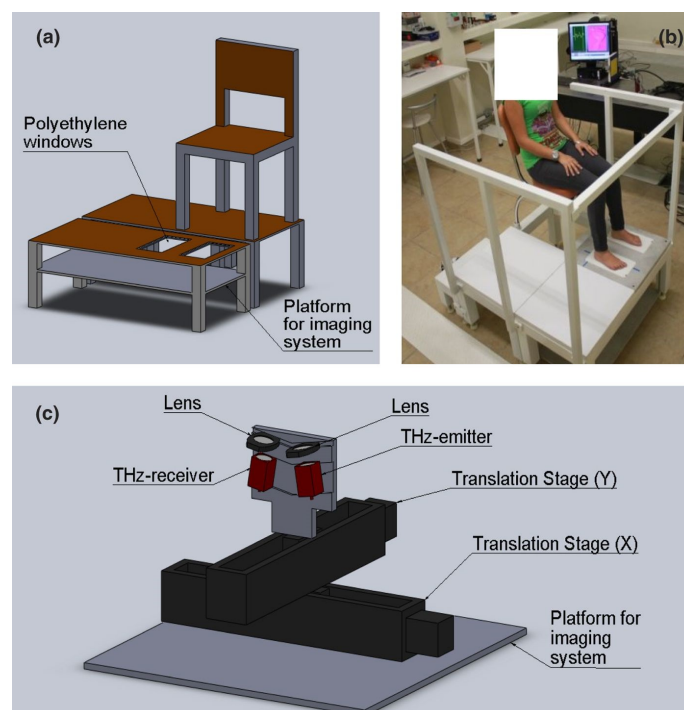


**Figure 6.** Platform for early screening of diabetic foot syndrome [204]. (a) THz setup design. It consists of an elevated surface where two high-density polyethylene windows are used to place the patient's feet. A chair is also provided in order to maintain the patient's position and avoid motion of the feet during the diagnostic image acquisition. The space under the patient sitting area is used to place the THz-TDS spectrometer and a raster scanning system [204]. (b) Photograph of the assembled setup during the testing. (c) Schematic layout of the raster-scanning imaging system, placed on the platform under the windows as indicated in (a).

Concerning brain tumors, Ji et al. in Figure 7 and in [205] demonstrated the effectiveness of THz reflectometry imaging (TRI) in distinguishing cancer and normal regions within a brain tissue section.

Relatively high intensity regions (depicted in red) are spatially well correlated to the tumor areas found with green fluorescent protein (GFP) and Hematoxylin and eosin (H&E) techniques.

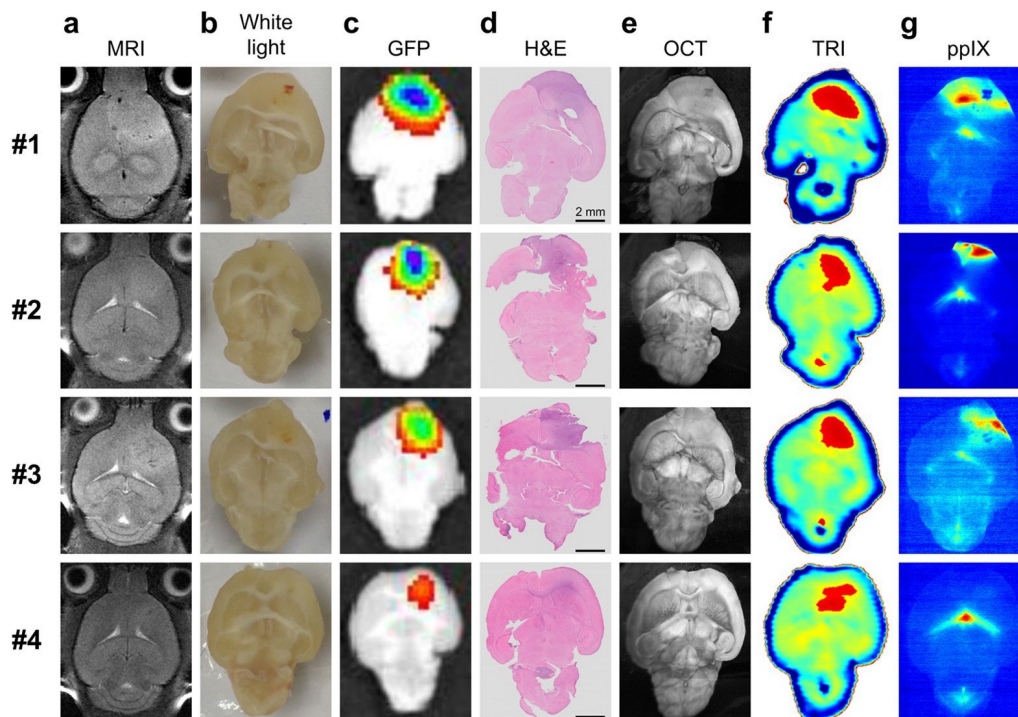


**Figure 7.** Brain tumor discrimination with different imaging techniques [205]. (a) MRI (magnetic resonance imaging). (b) White light imaging. (c) GFP (green fluorescent protein) imaging. (d) H&E (Hematoxylin and eosin) stained imaging. (e) OCT (optical coherence tomography) imaging. (f) THz reflectometry imaging (TRI). (g) 5-ALA-induced ppIX fluorescence imaging. TRI images show red regions (relatively high intensity) that are in agreement with tumor regions images obtained with GFP and H&E modalities, while in white light images, cancer regions are not identified.

Yamaguchi et al. [39], instead, take advantage of different optical properties (like refractive indexes and absorption coefficients) in normal and tumor regions to produce a THz image of a fresh rat brain tissue sample, see Figure 8.

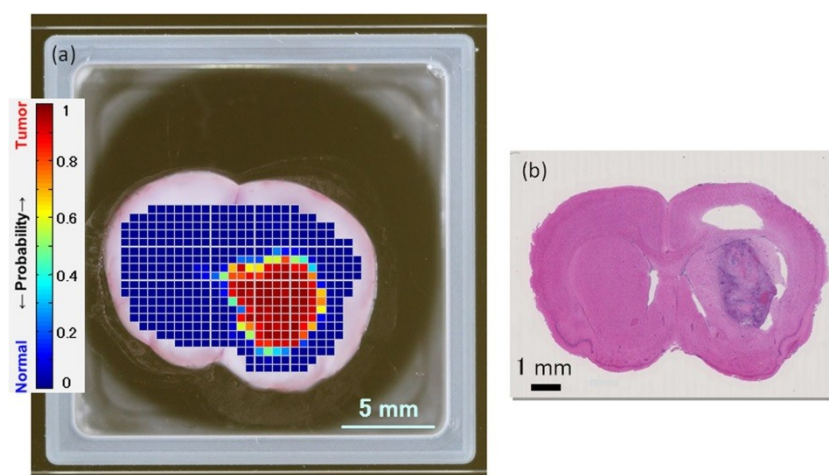


**Figure 8.** Brain tumor images of rat fresh tissue using different techniques: (a) THz spectroscopy and (b) HE-stained (hematoxylin and eosin) image of the same tissue section [39]. The THz image has been realized by computing a Tumor probability, where zero value corresponds to healthy tissue, based on the different refractive indexes of tumor and normal tissue regions. The red area in (a) shows the tumor region and is well in agreement with the dark purple area in HE-stained image (b).

Figure 8a shows the THz image based on the refractive index information (expressed as tumor probability), that results higher in the tumor than in the normal region (see also Figure 5). The red area locates the diseased tissue with great accordance to the HE-stained (hematoxylin and eosin) image of the same tissue section, where a darker purple region is visible (Figure 8b) [39].

Table 2 summarizes the main kind of tumor studied with TPI, with their relative references. Most works are ex vivo, while some papers for skin cancer are available in vivo and in vitro too.

**Table 2.** Different kind of tumors investigated with TPI and their references.

Tumor	Sample Status	References
Liver	<i>Ex vivo</i>	[173,174]
Brain-cervical	<i>Ex vivo</i>	[39,156,157,177,205,206]
Breast	<i>Ex vivo</i>	[132,163,172,179,181,187–190,192,195]
Oral-gastric-intestinal	<i>Ex vivo</i>	[154,161,162,164–166,176,180,185,186,207–210]
Skin	<i>In vivo</i>	[159,182–184,193,194]
	<i>In vitro</i>	
Ovarian	<i>Ex vivo</i>	[167]

Additionally, THz radiation is [211] a non-ionizing one, such that it is biologically safe for in vivo applications [212]. Moreover, the limited penetration depth of THz radiation has focused medical imaging research into the dentistry area [213]. TPI has been found to be an interesting technique for dental tissue (enamel, dentine and pulp) discrimination because refractive index differences enable the three tissue regions to be identified [66,148,214–217]. TPI is not the only possible technique for dental disease monitoring [218]: (i) visual caries examination, for example, loss of enamel translucency in the region between the contacting proximal surfaces of two adjacent teeth, (ii) X-ray imaging, (iii) electrical impedance measurements, (iv) ultrasound and (v) fluorescence-based methods [218,219] can also be adopted. However, many disadvantages can be assessed to some of these techniques: (i) is not possible at early detection stages, (i) and (ii) are difficult for posterior teeth, (ii) is potentially harmful for patients’ health because it uses ionizing radiation. For these reasons, additional strategies for dental health monitoring, with a particular emphasis on diagnosis at an earlier stage of formation and the use of non-ionizing radiations, are widely requested [218].

Arnone et al. used TPI in order to distinguish different animal and human tissues, in particular enamel, dentine and pulp, in human teeth. They realized two different kind of images with the same data set: TOF and absorption images. Being enamel ~99% mineral and dentine ~70% mineral, they show different refractive indexes, that result in different THz TOFs. The produced TOF image shows enamel only and enamel and dentine regions. In the absorption image, instead, the inner pulp region of tooth is visible, because it shows a strong absorption, thanks to the additional material in that tooth area [214]. Zinov'eva et al. [215] did some transmission images of human permanent molar tooth slices, at different THz frequencies, ranging from 0.2 to 1.5 THz. The teeth used in the experiments were processed to produce artificial lesions by chemical demineralization. The images clearly resolved enamel and dentine areas. In addition, demineralized tooth regions have shown an increase of THz transmission signal in comparison with healthy tooth tissue. This difference can be used to trace demineralization development in dental tissues [215]. Artificial demineralization detection has been the first step towards dental caries detection because caries regions are the result of mineral loss from enamel, causing a change in enamel refractive indexes and absorption coefficients. These changes can be exploited to identify lesions not visible to the naked eye. Early detection is important because initial stages of demineralization are reversible [66,148]. Crawley et al. [148] calculated enamel, dentine and caries absorption coefficients and refractive indexes in the range between 0.3 and 2.0 THz, in THz transmission geometry. Like [214], they produced a THz absorption map in a 210  $\mu\text{m}$  thick tooth slice and a TOF image, but with more accurate spatial resolution. Caries are correctly detected by the absorption image because average absorption coefficient of carious enamel is typically 35% larger than the one associated with healthy enamel, in that frequency range, using TPI. Enamel and dentine are precisely identified using TOF data because they are related to different refractive indexes. In reflection geometry, instead, some images have been created by plotting the change in THz pulse height at a specific time delay after reflection from the sample surface. In these images, both caries are detected, and dentine and enamel are differentiated. Moreover, they investigated a hypomineralization region of a 200  $\mu\text{m}$  thick tooth slice and demonstrated that TPI images can distinguish hypomineralization from enamel caries (demineralization) [216]. Finally, they demonstrated that even a TPI image of a tooth hemisection (much thicker with respect to previous slices) can discriminate caries inside it.

A 3D study of dental tissue has been reported in [217]. The enamel-dentine junction in 12 human incisor teeth has been detected in 91% of the cases. A series of ~100  $\mu\text{m}$  deep steps were chemically produced in order to alter enamel thickness. They were imaged and the authors demonstrated that they accurately and reliably make direct measurements of enamel thickness; this is necessary for monitoring enamel erosion, a common dental disorder.

Finally, in order to verify TPI validity and effectiveness in dental caries detection, Kamburoğlu et al. [218] compared TPI (static images and movie video) with common radiological techniques: intraoral photostimulable phosphor plate (PSP) and cone beam CT (CBCT) for the detection of dental caries *ex vivo* [218–220]. They demonstrated that TPI shows good performances for caries identification, compared to the most used techniques, see Figure 9.

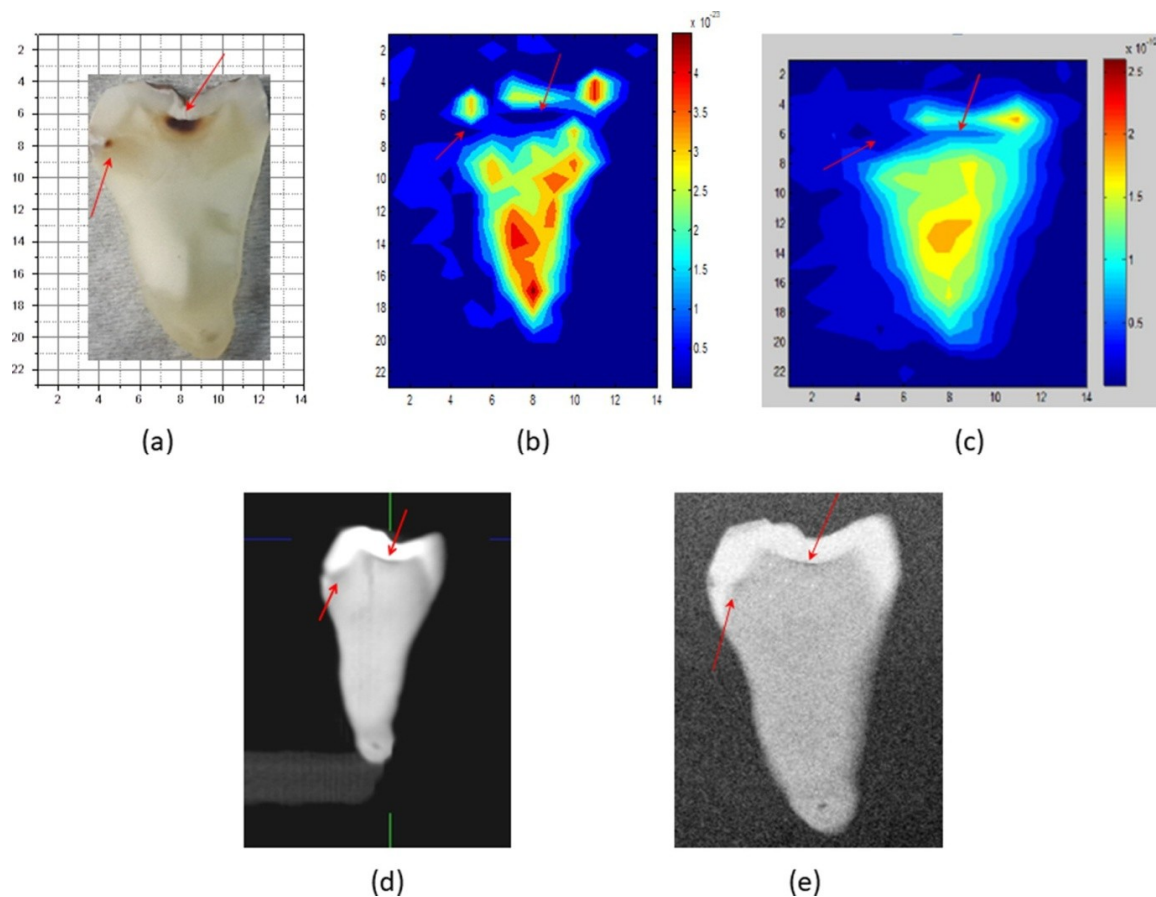


**Figure 9.** Tooth caries identification with different imaging techniques [218]. (a) White light image. (b) THz static image at 0.35 THz. (c) THz image from video movie. (d) CBCT (cone beam CT) image. (e) PSP (photostimulable phosphor plate) image. Red arrows indicate dental caries in tooth tissue. The five images are in agreement in identifying caries regions.

## 5. Conclusions

In summary, the rapid THz technological advances have led THz radiation to emerge as a promising and useful tool in medicine. We have outlined the detection techniques of THz pulsed radiation and biomedical applications, based on the use of TPI systems.

In this perspective, we have summarized the prominent advantages in the use of THz radiation, with particular attention to THz pulsed radiation. Briefly, we have illustrated THz pulsed sources, and subsequently incoherent and coherent detectors, that are commercially available and/or of interest for technological research. The common schematic layouts for reflection and transmission imaging modes are discussed too.

Concerning the THz radiation properties, we have discussed the major application of TPI in the field of biomedicine, reporting many examples of *ex vivo* and *in vivo* studies, including cases of histopathological imaging of cancers, which are suitable targets. The enhancement of the sensing capabilities and penetration depth within tissues, in medical applications, were addressed. This represents a delicate point to question, and in particular the use of PEAs should require more attention, and many extended trials should be carried out to allow the application of TPI systems in clinical fields and hospitals.

Although THz technology is rapidly increasing as a medical imaging modality, and THz imaging applications in biomedical fields have drawn extensive interest, the technologies are maturing and the principles have been demonstrated in order to direct efforts towards the realization that THz clinical applications are viable in the real world.

**Author Contributions:** Writing-Original Draft Preparation, A.D. and M.D.F.; Writing-Review & Editing, all authors; Formal Analysis, M.D.F. and V.D.; Supervision, S.L. and M.P.; Project Administration, S.L.; Funding Acquisition, S.L. All authors have read and agreed to the published version of the manuscript.

**Funding:** We acknowledge the financial support of the Bilateral Cooperation Agreement between Italy and Japan of the Italian Ministry of Foreign Affairs and of the International Cooperation (MAECI), in the framework of the project of major relevance N. PGR00728.

**Conflicts of Interest:** The authors declare no conflict of interest.

## References

1. Cao, Q.; Zhegalova, N.; Wang, S.; Akers, W.; Berezin, M. Multispectral imaging in the extended near-infrared window based on endogenous chromophores. *J. Biomed. Opt.* **2013**, *18*, 101318. [[CrossRef](#)] [[PubMed](#)]
2. Wilson, R.; Nadeau, K.; Jaworski, F.; Rowland, R.; Nguyen, J.; Crouzet, C.; Saager, R.; Choi, B.; Tromberg, B.; Durkin, A. Quantitative short-wave infrared multispectral imaging of in vivo tissue optical properties. *J. Biomed. Opt.* **2014**, *19*, 086011. [[CrossRef](#)] [[PubMed](#)]
3. Bazylewski, P.; Ezugwu, S.; Fanchini, G. A review of Three-Dimensional Scanning Near-Field Optical Microscopy (3D-SNOM) and Its Applications in Nanoscale Light Management. *Appl. Sci.* **2017**, *7*, 973. [[CrossRef](#)]
4. Weng, Q.; Panchai, V.; Lin, K.T.; Sun, L.; Kajihara, Y.; Tzalenchuk, A.; Komiyama, S. Comparison of active and passive methods for the infrared scanning near-field microscopy. *Appl. Phys. Lett.* **2019**, *114*, 153101. [[CrossRef](#)]
5. Jeon, S.; Kim, J.; Lee, D.; Baik, J.W.; Kim, C. Review on practical photoacoustic microscopy. *Photoacoustics* **2019**, *15*, 100141. [[CrossRef](#)]
6. Guo, R.; Lu, G.; Qin, B.; Fe, B. Ultrasound Imaging Technologies for Breast Cancer Detection and Management: A Review. *Ultrasound Med. Biol.* **2018**, *44*, 37–70. [[CrossRef](#)]
7. Xu, C.; Carney, P.S.; Boppart, S.A. Wavelength-dependent scattering in spectroscopic optical coherence tomography. *Opt. Express* **2005**, *13*, 450–462. [[CrossRef](#)]
8. Xu, C.; Vinegoni, C.; Ralston, T.S.; Luo, W.; Tan, W.; Boppart, S.A. Spectroscopic spectral-domain optical coherence microscopy. *Opt. Lett.* **2006**, *31*, 1079–1081. [[CrossRef](#)]
9. Kim, M.K. Principles and techniques of digital holographic microscopy. *SPIE Rev.* **2010**, *1*, 018005. [[CrossRef](#)]
10. Marquet, P.; Depeursinge, C.; Magistretti, P.J. Review of quantitative phase-digital holographic microscopy: Promising novel imaging technique to resolve neuronal network activity and identify cellular biomarkers of psychiatric disorders. *Neurophotonics* **2014**, *1*, 020901. [[CrossRef](#)]
11. Pitkäaho, T.; Manninen, A.; Naughton, T.J. Focus prediction in digital holographic microscopy using deep convolutional neural networks. *Appl. Opt.* **2019**, *58*, A202–A208. [[CrossRef](#)] [[PubMed](#)]
12. Jermyn, M.; Mok, K.; Mercier, J.; Desroches, J.; Pichette, J.; Saint-Arnaud, K.; Bernstein, L.; Guiot, M.C.; Petrecca, K.; Leblond, F. Intraoperative brain cancer detection with Raman spectroscopy in humans. *Sci. Transl. Med.* **2015**, *7*, 274ra19. [[CrossRef](#)] [[PubMed](#)]
13. Min, W.; Freudiger, C.W.; Lu, S.; Xie, X.S. Coherent Nonlinear Optical Imaging: Beyond Fluorescence Microscopy. *Annu. Rev. Phys. Chem.* **2011**, *62*, 507–530. [[CrossRef](#)] [[PubMed](#)]
14. Zumbusch, A.; Langbein, W.; Borri, P. Nonlinear vibrational microscopy applied to lipid biology. *Prog. Lipid. Res.* **2013**, *52*, 615–632. [[CrossRef](#)] [[PubMed](#)]
15. Zhang, C.; Zhang, D.; Cheng, J.X. Coherent Raman Scattering Microscopy in Biology and Medicine. *Annu. Rev. Biomed. Eng.* **2015**, *17*, 415–445. [[CrossRef](#)] [[PubMed](#)]
16. D'Arco, A.; Brancati, N.; Ferrara, M.A.; Indolfi, M.; Frucci, M.; Sirleto, L. Subcellular chemical and morphological analysis by stimulated Raman scattering microscopy and image analysis techniques. *BOE* **2016**, *7*, 1853–1864.
17. Cheng, J.X.; Xie, X.S. Vibrational spectroscopic imaging of living systems: An emerging platform for biology and medicine. *Science* **2015**, *350*, aaa8870. [[CrossRef](#)]
18. Lu, F.K.; Calligaris, D.; Olibiyi, O.I.; Norton, I.; Yang, W.; Santagata, S.; Xie, X.S.; Golby, A.J.; Agar, N.Y.R. Label-Free Neurosurgical pathology with Stimulated Raman Imaging. *Cancer Res.* **2016**, *76*, OF1–OF12. [[CrossRef](#)] [[PubMed](#)]

19. Oheim, M.; Michael, D.J.; Geisbauer, M.; Madsen, D.; Chow, R.H. Principles of two-photon excitation fluorescence microscopy and other nonlinear imaging approaches. *Adv. Drug Deliv. Rev.* **2006**, *58*, 788–808. [[CrossRef](#)]
20. Müller, M.; Zumbusch, A. Coherent anti-Stokes Raman Scattering Microscopy. *Chem. Phys. Chem.* **2007**, *8*, 2156–2170. [[CrossRef](#)]
21. Li, J.; Chen, Q.; Sun, J.; Zhang, J.; Ding, J.; Zuo, C. Three-dimensional tomographic microscopy technique with multi-frequency combination with partially coherent illuminations. *BOE* **2018**, *9*, 2526–2542. [[CrossRef](#)] [[PubMed](#)]
22. Li, J.; Lin, P.; Tan, Y.; Cheng, J.X. Volumetric stimulated Raman scattering imaging of cleared tissues towards three-dimensional chemical histopathology. *BOE* **2019**, *10*, 4329. [[CrossRef](#)] [[PubMed](#)]
23. Orringer, D.A.; Pandian, B.; Niknafs, Y.S.; Hollon, T.C.; Boyle, J.; Lewis, S.; Garrard, M.; Hervey-Jumper, S.L.; Garton, H.J.L.; Maher, C.O.; et al. Rapid intraoperative histology of unprocessed surgical specimens via fibre-laser-based stimulated Raman scattering microscopy. *Nat. Biomed. Eng.* **2017**, *1*, 0027. [[CrossRef](#)]
24. Denk, W.; Strickler, J.H.; Webb, W.W. Two-photon laser scanning fluorescence microscopy. *Science* **1990**, *248*, 73–76. [[CrossRef](#)] [[PubMed](#)]
25. Cicchi, R.; Kapsokalyvas, D.; Pavone, F.S. Clinical Nonlinear Laser Imaging of Human Skin: A Review. *Biomed. Res. Int.* **2014**, *2014*, 903589. [[CrossRef](#)] [[PubMed](#)]
26. Campagnola, P.J.; Loew, L.M. Second-harmonic imaging microscopy for visualizing biomolecular arrays in cells, tissues and organisms. *Nat. Biotechnol.* **2003**, *21*, 1356–1360. [[CrossRef](#)]
27. Miller, D.R.; Jarrett, J.W.; Hassan, A.M.; Dunn, A.K. Deep tissue imaging with multiphoton fluorescence microscopy. *Curr. Opin. Biomed. Eng.* **2017**, *4*, 32–39. [[CrossRef](#)]
28. Castello, M.; Tortarolo, G.; Buttafava, M.; Deguchi, T.; Villa, F.; Koho, S.; Pesce, L.; Oneto, M.; Pelicci, S.; Lanzanò, L.; et al. A robust and versatile platform for imaging scanning microscopy enabling super-resolution FLIM. *Nat. Methods* **2019**, *16*, 175–178. [[CrossRef](#)]
29. Müller, T.; Schumann, C.; Kraegeloh, A. STED Microscopy and its Applications: New Insights into Cellular Processes on the Nanoscale. *Chem. Phys. Chem.* **2012**, *13*, 1986–2000. [[CrossRef](#)]
30. Huang, B.; Babcock, H.; Zhuang, X. Breaking the Diffraction Barrier: Super-Resolution Imaging of Cells. *Cell* **2010**, *143*, 1047–1058. [[CrossRef](#)]
31. Pietraszewska-Bogiel, A.; Gadella, T.W.J. FRET microscopy: From principle to routine technology in cell biology. *J. Microsc.* **2011**, *241*, 111–118. [[CrossRef](#)] [[PubMed](#)]
32. Auston, D.H.; Nuss, M.C. Electrooptical generation and detection of femtosecond electrical transients. *IEEE J. Quantum Electron.* **1988**, *24*, 184–197. [[CrossRef](#)]
33. Mittleman, D.; Gupta, M.; Neelamani, R.; Baraniuk, R.G.; Rudd, J.V.; Koc, M. Recent advances in terahertz imaging. *Appl. Phys. B* **1999**, *68*, 1085–1094. [[CrossRef](#)]
34. Siegel, P.H. Terahertz technology in biology and medicine. *IEEE Trans. Microw. Theory* **2004**, *52*, 2438–2447. [[CrossRef](#)]
35. Zhang, X.C. Terahertz wave imaging: Horizons and hurdles. *Phys. Med. Biol.* **2002**, *47*, 3667–3677. [[CrossRef](#)]
36. Wallace, V.P.; Taday, P.F.; Fitzgerald, A.J.; Woodward, R.M.; Cluff, J.; Pye, R.J.; Arnone, D.D. Terahertz pulsed imaging and spectroscopy for biomedical and pharmaceutical applications. *Faraday Discuss* **2004**, *126*, 255–263. [[CrossRef](#)]
37. Withayachumnankul, W.; Png, G.M.; Yin, X.; Atakramians, S.; Jones, I.; Lin, H.; Ung, B.S.Y.; Balakrishnan, J.; Ng, B.W.-H.; Ferguson, B.; et al. T-ray sensing and imaging. *Proc. IEEE* **2007**, *95*, 1528–1558. [[CrossRef](#)]
38. Mickan, S.; Abbott, D.; Munchb, J.; Zhang, X.C.; van Doorn, T. Analysis of system trade-offs for terahertz imaging. *Microelectron. J.* **2000**, *31*, 503–514. [[CrossRef](#)]
39. Yamaguchi, S.; Yamaguchi, S.; Fukushi, Y.; Kubota, O.; Itsuji, T.; Ouchi, T.; Yamamoto, S. Brain tumor imaging of rat fresh tissue using terahertz spectroscopy. *Sci. Rep.* **2016**, *6*, 30124. [[CrossRef](#)]
40. Bajwa, N.; Au, J.; Jarrahy, R.; Sung, S.; Fishbein, M.C.; Riopelle, D.; Ennis, D.B.; Aghaloo, T.; John, M.A.; Grundfest, W.S.; et al. Non-invasive terahertz imaging of tissue water content for flap viability assessment. *BOE* **2017**, *8*, 460–474. [[CrossRef](#)]
41. Karagoz, B.; Altan, H.; Kamburoglu, K. Terahertz pulsed imaging study of dental caries. In *Medical Laser Applications and Laser-tissue Interactions VII. Proceedings of the European Conference on Biomedical Optics, Optical Society of America, Munich, Germany, 21–25 June 2015*; Lilge, L., Sroka, R., Eds.; SPIE: Washington, NY, USA, 2015; Volume 9542, 95420N.

42. Zaytsev, I.; Dolganova, I.N.; Chernomyrdin, N.V.; Katyba, G.M.; Gavdush, A.A.; Cherkasova, O.P.; Komandin, G.A.; Shchedrina, M.A.; Khodan, A.N.; Ponomarev, D.S.; et al. The progress and perspectives of terahertz technology for diagnosis of neoplasms: A review. *J. Opt.* **2020**, *22*, 013001. [[CrossRef](#)]
43. Yang, X.; Zhao, X.; Yang, K.; Liu, Y.; Liu, Y.; Fu, W.; Luo, Y. Biomedical Applications of Terahertz Spectroscopy and Imaging. *Trends Biotechnol.* **2016**, *34*, 810–824. [[CrossRef](#)] [[PubMed](#)]
44. Son, J.H.; Oh, S.J.; Cheon, H. Potential clinical applications of terahertz radiation. *J. Appl. Phys.* **2019**, *125*, 190901. [[CrossRef](#)]
45. Leahy-Hoppa, M.R.; Miragliotta, J.; Osiander, R.; Burnett, J.; Dikmelik, Y.; McEnnis, C.; Spicer, J.B. Ultrafast Laser-Based Spectroscopy and Sensing: Applications in LIBS, CARS, and THz Spectroscopy. *Sensors* **2010**, *10*, 4342–4372. [[CrossRef](#)] [[PubMed](#)]
46. Fischer, B.; Hoffmann, M.; Helm, H.; Modjesch, G.; Uhd Jepsen, P. Chemical recognition in terahertz time-domain spectroscopy and imaging. *Semicond. Sci. Technol.* **2005**, *20*, S246. [[CrossRef](#)]
47. D’Arco, A.; Di Fabrizio, M.; Dolci, V.; Marcelli, A.; Petrarca, M.; Della Ventura, G.; Lupi, S. Characterization of volatile organic compounds (VOCs) in their liquid-phase by terahertz time-domain spectroscopy. *BOE* **2020**, *11*, 1–7. [[CrossRef](#)] [[PubMed](#)]
48. Stoik, C.D.; Bohn, M.J.; Blackshire, J.L. Nondestructive evaluation of aircraft composites using transmissive terahertz time domain spectroscopy. *Opt. Express* **2008**, *16*, 17039–17051. [[CrossRef](#)] [[PubMed](#)]
49. Heimbeck, M.S.; Ng, W.R.; Golish, D.R.; Gehm, M.E.; Everitt, H.O. Terahertz digital holographic imaging of voids within visibly opaque dielectrics. *IEEE Trans. Terahertz Sci. Technol.* **2015**, *5*, 110–116. [[CrossRef](#)]
50. Giuliano, B.M.; Gavdush, A.A.; Müller, B.; Zaytsev, K.I.; Grassi, T.; Ivlev, A.V.; Palumbo, M.E.; Baratta, G.A.; Scirè, C.; Komandin, G.A.; et al. Broadband spectroscopy of astrophysical ice analogues I. Direct measurement of the complex refractive index of CO ice using terahertz time-domain spectroscopy. *Astron. Astrophys.* **2019**, *629*, A112. [[CrossRef](#)]
51. Federici, J.F.; Schulkin, B.; Huang, F.; Gary, D.; Barat, R.; Oliveira, F.; Zimdars, D. THz imaging and sensing for security applications—Explosives, weapons and drugs. *Semicond. Sci. Technol.* **2005**, *20*, S266. [[CrossRef](#)]
52. Ergün, S.; Sönmez, S. Terahertz Technology for Military Applications. *J. Assoc. Inf. Sci. Technol.* **2015**, *3*, 13–16. [[CrossRef](#)]
53. Liu, H.B.; Zhong, H.; Karpowicz, N.; Chen, Y.; Zhang, X.C. Terahertz spectroscopy and imaging for defense and security applications. *Proc. IEEE* **2007**, *95*, 1514–1527. [[CrossRef](#)]
54. Wang, K.; Sun, D.W.; Pu, H. Emerging non-destructive terahertz spectroscopic imaging technique: Principle and applications in the agri-food industry. *Trend Food Sci. Technol.* **2017**, *67*, 93–105. [[CrossRef](#)]
55. Cosentino, A. Terahertz and cultural heritage science: Examination of art and archeology. *Technologies* **2016**, *4*, 6. [[CrossRef](#)]
56. Lee, Y.S. *Principles of Terahertz Science and Technology*; Springer: Berlin/Heidelberg, Germany, 2009.
57. Zhang, X.C.; Xu, J. *Introduction to THz Wave Photonics*; Springer: Berlin/Heidelberg, Germany, 2010.
58. Manti, L.; D’Arco, A. Cooperative biological effects between ionizing radiation and other physical and chemical agents. *Mutat. Res.* **2010**, *704*, 115–122. [[CrossRef](#)]
59. Titova, L.V.; Rodriguez-Juarez, R.; Woycicki, R.; Hegmann, F.A.; Kovalchuk, O. Intense THz pulses down-regulate genes associated with skin cancer and psoriasis: A new therapeutic avenue? *Sci. Rep.* **2013**, *3*, 2363. [[CrossRef](#)] [[PubMed](#)]
60. Fëdorov, V.I.; Serdyukov, D.S.; Cherkasova, O.P.; Popova, S.S.; Nemova, E.F. The influence of terahertz radiation on the cell’s genetic apparatus. *J. Opt. Technol.* **2017**, *84*, 509–514. [[CrossRef](#)]
61. Naftaly, M. (Ed.) *Terahertz Metrology*; Artech House: London, UK, 2015.
62. Chevalier, P.; Amirzhan, A.; Wang, F.; Piccardo, M.; Johnson, S.G.; Capasso, F.; Everitt, H.O. Widely tunable compact terahertz gas lasers. *Science* **2019**, *366*, 856–860. [[CrossRef](#)]
63. Otsuji, T. Trends in the research of modern terahertz detectors: Plasmon detectors. *IEEE Trans. Terahertz Sci. Technol.* **2015**, *5*, 1110–1120.
64. Hu, B.B.; Nuss, M.C. Imaging with terahertz waves. *Opt. Lett.* **1995**, *20*, 1716–1718. [[CrossRef](#)]
65. Walther, M.; Fischer, B.M.; Ortner, A.; Bitzer, A.; Thoman, A.; Helm, H. Chemical sensing and imaging with pulsed terahertz radiation. *Anal. Bioanal. Chem.* **2010**, *397*, 1009–1017. [[CrossRef](#)] [[PubMed](#)]
66. Pickwell, E.; Wallace, V.P. Biomedical applications of terahertz technology. *J. Phys. D Appl. Phys.* **2006**, *39*, R301–R310. [[CrossRef](#)]

67. Auston, D.H. Picosecond optoelectronic switching and gating in silicon. *Appl. Phys. Lett.* **1975**, *26*, 101–103. [[CrossRef](#)]
68. Grischkowsky, D.; Keiding, S.; van Exter, M.; Fittinger, C.H. Far-infrared time-domain spectroscopy with terahertz beams of dielectrics and semiconductors. *J. Opt. Soc. Am. B* **1990**, *7*, 2006–2015. [[CrossRef](#)]
69. Tani, M.; Herrmann, M.; Sakai, K. Generation and detection of terahertz pulsed radiation with photoconductive antennas and its application to imaging. *Meas. Sci. Technol.* **2002**, *13*, 1739–1745. [[CrossRef](#)]
70. Zhang, X.C.; Ma, X.F.; Jin, Y.; Lu, T.M.; Boden, E.P.; Phelp, P.D.; Stewart, K.R.; Yakymyshyn, C.P. Terahertz optical rectification from a nonlinear organic crystal. *Appl. Phys. Lett.* **1992**, *61*, 3080–3082. [[CrossRef](#)]
71. Wu, Q.; Zhang, X.C. Terahertz broadband GaP electro-optic sensor. *Appl. Phys. Lett.* **1997**, *70*, 1784. [[CrossRef](#)]
72. Winnewisser, C.; Jepsen, P.; Schall, M.; Schyja, V.; Helm, H. Electro-optic detection of THz radiation in LiAlO<sub>3</sub>, LiNbO<sub>3</sub> and ZnTe. *Appl. Phys. Lett.* **1997**, *70*, 3069. [[CrossRef](#)]
73. Kim, K.Y.; Taylor, A.J.; Glowina, J.H.; Rodriguez, G. Coherent control of terahertz supercontinuum generation in ultrafast laser-gas interactions. *Nat. Photonics* **2008**, *2*, 605–609. [[CrossRef](#)]
74. Thomson, M.D.; Blank, V.; Roskos, H.G. Terahertz white-light pulses from an air plasma photo-induced by incommensurate two-color optical fields. *Opt. Express* **2010**, *18*, 23173–23182. [[CrossRef](#)]
75. Dai, J.; Liu, J.; Zhang, X.C. Terahertz wave air photonics: Terahertz wave generation and detection with laser-induced gas plasma. *IEEE J. Sel. Top. Quantum Electron.* **2011**, *17*, 183–190. [[CrossRef](#)]
76. Planken, P.C.M.; Nuss, M.C.; Knox, W.H.; Miller, D.A.B.; Goossen, K.W. THz pulses from the creation of polarized electron-hole pairs in biased quantum wells. *Appl. Phys. Lett.* **1992**, *61*, 2009–2011. [[CrossRef](#)]
77. Sun, G.; Xu, G.; Ding, Y.J.; Zhao, H.; Liu, G.; Zhang, J.; Tansu, N. Efficient Terahertz Generation Within InGaN/GaN Multiple Quantum Wells. *IEEE J. Sel. Top. Quantum Electron.* **2011**, *17*, 48–53. [[CrossRef](#)]
78. Roskos, H.G.; Nuss, M.C.; Shah, J.; Leo, K.D.; Miller, A.; Fox, A.M.; Schmitt-Rink, S.; Köhler, K. Coherent submillimeter-wave emission from charge oscillations in a double-well potential. *Appl. Phys. Lett.* **1992**, *68*, 2216–2219. [[CrossRef](#)] [[PubMed](#)]
79. Huber, R.; Brodshelm, A.; Tauser, F.; Leitenstorfer, A. Generation and field-resolved detection of femtosecond electromagnetic pulses tunable up to 41 THz. *Appl. Phys. Lett.* **2000**, *76*, 3191–3193. [[CrossRef](#)]
80. Kono, S.; Tani, M.; Sakai, K. Ultrabroadband Photoconductive Detection: Comparison with Free-Space Electro-Optic Sampling. *Appl. Phys. Lett.* **2001**, *79*, 898–900. [[CrossRef](#)]
81. Houver, S.; Huber, L.; Savoini, M.; Abreu, E.; Johnson, S.L. 2D THz spectroscopic investigation of ballistic conduction-band electron dynamics in InSb. *Opt. Express* **2019**, *27*, 10854. [[CrossRef](#)]
82. Curcio, A.; Dolci, V.; Lupi, S.; Petrarca, M. Terahertz-based retrieval of the spectral phase and amplitude of ultrashort laser pulses. *Opt. Lett.* **2018**, *43*, 783. [[CrossRef](#)]
83. Liu, B.; Bromberger, H.; Cartella, A.; Gebert, T.; Först, M.; Cavalleri, A. Generation of narrowband, high-intensity, carrier-envelope phase-stable pulses tunable between 4 and 18 THz. *Opt. Lett.* **2017**, *42*, 129. [[CrossRef](#)]
84. Zhang, Y.; Zhang, X.; Li, S.; Gu, J.; Li, Y.; Tian, Z.; Ouyang, C.; He, M.; Hanand, J.; Zhang, W. Broadband THz-TDS System based on DSTMS emitter and LTGInGaAs/InAlAs Photoconductive Antenna Detector. *Sci. Rep.* **2016**, *6*, 26949. [[CrossRef](#)]
85. Jazbinšek, M.; Puc, U.; Abina, A.; Zidansek, A. Organic crystals for THz photonics. *Appl. Sci.* **2019**, *9*, 882. [[CrossRef](#)]
86. Hebling, J.; Yeh, K.L.; Hoffmann, M.C.; Bartal, B.; Nelson, K.A. Generation of High-Power Terahertz Pulses by Tilted-Pulse-Front Excitation and Their Application Possibilities. *J. Opt. Soc. Am. B* **2008**, *25*, B6–B19. [[CrossRef](#)]
87. Hamster, H.; Sullivan, A.; Gordon, S.; White, W.; Falcone, R.W. Subpicosecond Electromagnetic Pulses from Intense Laser-Plasma Interaction. *Phys. Rev. Lett.* **1993**, *71*, 2725. [[CrossRef](#)] [[PubMed](#)]
88. Hamster, H.; Sullivan, A.; Gordon, S.; Falcone, R.W. Short-Pulse Terahertz Radiation from High-Intensity-Laser-Produced Plasmas. *Phys. Rev. E* **1994**, *49*, 671. [[CrossRef](#)]
89. Löffler, T.; Jacob, F.; Roskos, H.G. Generation of terahertz pulses by photoionization of electrically biased air. *Appl. Phys. Lett.* **2000**, *77*, 453–455. [[CrossRef](#)]
90. Cook, D.J.; Hochstrasser, R.M. Intense terahertz pulses by four-wave rectification in air. *Opt. Lett.* **2000**, *25*, 1210–1212. [[CrossRef](#)]

91. Schmuttenmaer, C.A. Exploring dynamics in the far-infrared with terahertz spectroscopy. *Chem. Rev.* **2004**, *104*, 1759–1780. [[CrossRef](#)]
92. Greene, B.I.; Federici, J.F.; Dykaar, D.R.; Levi, A.F.J.; Pfeiffer, L. Picosecond pump and probe spectroscopy utilizing freely propagating terahertz radiation. *Opt. Lett.* **1991**, *16*, 48–49. [[CrossRef](#)]
93. Gouider, F.; Vasilyev, Y.B.; Bugár, M.; Könnemann, J.; Buckle, P.D.; Nachtwei, G. Terahertz photoresponse of AlInSb/InSb/AlInSb quantum well structures. *Phys. Rev. B* **2010**, *81*, 155304. [[CrossRef](#)]
94. Oda, N. Uncooled bolometer-type terahertz focal plane array and camera for real-time imaging. *C. R. Phys.* **2010**, *11*, 496–509. [[CrossRef](#)]
95. Dean, P.; Shaukat, M.U.; Khanna, S.P.; Lachab, M.; Burnett, A.; Davies, A.G.; Linfield, E.H.; Chakraborty, S. Absorption-sensitive diffuse reflection imaging of concealed powders using a terahertz quantum cascade laser. *Opt. Express* **2008**, *16*, 5997–6007. [[CrossRef](#)] [[PubMed](#)]
96. Golay, M.J.E. The theoretical and practical sensitivity of the pneumatic infrared detector. *Rev. Sci. Instrum.* **1949**, *20*, 816–820. [[CrossRef](#)] [[PubMed](#)]
97. Karpowicz, N.; Zhong, H.; Xu, J.; Lin, K.I.; Hwang, J.S.; Zhang, X.C. Comparison between pulsed terahertz time-domain imaging and continuous wave terahertz imaging. *Semicond. Sci. Technol.* **2005**, *20*, S293–S299. [[CrossRef](#)]
98. Cox, J.A.; Higashi, R.; Nusseibeh, F.; Newstrom-Peitso, K.; Zins, C. Uncooled MEMS-based detector arrays for THz imaging applications. In *Terahertz Physics, Devices, and Systems III: Advanced Applications in Industry and Defense, Proceedings of the SPIE Defense, Security, and Sensing, Orlando, FL, USA, 13–17 April 2009*; SPIE: Washington, NY, USA; Volume 7311, 73110R.
99. Kašalynas, I.; Adam, A.J.L.; Klaassen, O.; Hovenier, N.J.; Pandraud, G.; Iordanov, V.P.; Sarro, P.M. Some properties of a room temperature THz detection array. In *Advanced Optical Materials, Technologies, and Devices, Proceedings of the SPIE Advanced Optical Materials, Technologies, and Devices, Vilnius, Lithuania, 27–30 August 2006*; SPIE: Washington, NY, USA; Volume 6596, 65960J.
100. Semenov, A.; Cojocari, O.; Hübers, H.-W.; Song, F.; Klushin, A.; Müller, A.-S. Application of Zero-Bias Optical Schottky-Diode Detectors for Monitoring Short-Pulse and Weak Terahertz Radiation. *IEEE Electron Device Lett.* **2010**, *31*, 674–676. [[CrossRef](#)]
101. Maestrini, A.; Thomas, B.; Wang, H.; Jung, C.; Treuttel, J.; Jin, Y.; Chattopadhyay, G.; Mehdi, I.; Beaudin, G. Schottky diode-based terahertz frequency multipliers and mixers. *C. R. Phys.* **2010**, *11*, 480–495. [[CrossRef](#)]
102. Nazarov, M.M.; Makarova, S.A.; Shkurinov, A.P.; Okhotnikov, O.G. The use of combination of nonlinear optical materials to control terahertz pulse generation and detection. *Appl. Phys. Lett.* **2008**, *92*, 021114–021117. [[CrossRef](#)]
103. Zhang, Y.; Hosono, S.; Nagai, N.; Song, S.-H.; Hirakawa, K. Fast and sensitive bolometric terahertz detection at room temperature through thermomechanical transduction. *J. Appl. Phys.* **2019**, *125*, 151602. [[CrossRef](#)]
104. Rezvani, J.; Di Gioacchino, D.; Gatti, C.; Poccia, N.; Ligi, C.; Tocci, S.; Cestelli Guidi, M.; Cibella, S.; Lupi, S.; Marcelli, A. Tunable Vortex Dynamics in Proximity Junction Arrays: A Possible Accurate and Sensitive 2D THz Detector. In *Proceedings of the LIV Zakopane School of Physics, Breaking Frontiers, Zakopane, Poland, 21–25 May 2019*; Volume 137, pp. 17–20.
105. Knap, W.; Dyakonov, M.I. Field effect transistors for terahertz applications. In *Handbook of Terahertz Technology for Imaging, Sensing and Communications*; Volume in Woodhead Publishing Series in Electronics and Optical Materials; Saeedkia, D., Ed.; Elsevier: Amsterdam, The Nederland, 2013; pp. 121–155.
106. Fan, K.; Suen, J.Y.; Liu, X.; Padilla, W.J. All-dielectric metasurface absorbers for uncooled terahertz imaging. *Optica* **2017**, *4*, 601–604. [[CrossRef](#)]
107. Guerboukha, H.; Nallappan, K.; Skorobogatiy, M. Toward real-time terahertz imaging. *Adv. Opt. Phot.* **2018**, *10*, 843–938. [[CrossRef](#)]
108. Cho, H.; Lee, S.H.; Nam-Gung, C.; Oh, S.J.; Oh, J.H.; Park, H.; Ahn, C.B. Fast terahertz reflection tomography using block-based compressed sensing. *Opt. Express* **2011**, *19*, 16401–16409. [[CrossRef](#)]
109. Hwang, B.M.; Lee, S.H.; Lim, W.T.; Ahn, C.B.; Son, J.H.; Park, H. A fast spatial-domain terahertz imaging using block-based compressed sensing. *J. Infrared Millim. Terahertz Waves* **2011**, *32*, 1328–1336. [[CrossRef](#)]
110. Hong, H.J.; Park, J.; Park, H.; Son, J.H.; Ahn, C.B. Pre- and post-processing for tomographic reconstruction of terahertz time-domain spectroscopy. *Opt. Express* **2013**, *21*, 19943–19950. [[CrossRef](#)] [[PubMed](#)]

111. Wallace, V.P.; Macpherson, E.; Zeitler, J.A.; Reid, C. Three-dimensional imaging of optically opaque materials using nonionizing terahertz radiation. *J. Opt. Soc. Am. Opt. Image Sci. Vis.* **2008**, *25*, 3120–3133. [[CrossRef](#)] [[PubMed](#)]
112. Castro-Camus, E.; Alfaro, M. Photoconductive devices for terahertz pulsed spectroscopy: A review. *Photon. Res.* **2016**, *4*, A36. [[CrossRef](#)]
113. Chan, W.L.; Deibel, J.; Mittleman, D.M. Imaging with terahertz radiation. *Rep. Prog. Phys.* **2007**, *70*, 1325–1379. [[CrossRef](#)]
114. Adam, A.J.L. Review of Near-Field Terahertz Measurement Methods and Their Applications. *J. Infrared Millim. Terahertz Waves* **2011**, *32*, 976–1019. [[CrossRef](#)]
115. Goodman, J.W. *Introduction to Fourier Optics*, 2nd ed.; McGraw-Hill: New York, NY, USA, 1996.
116. Abbe, E. Beiträge zur theorie des mikroskops und der mikroskopischen wahrnehmung. *Arch. Mikrosk. Anat.* **1873**, *9*, 413–468. [[CrossRef](#)]
117. Born, M.; Wolf, E. *Principles of Optics*, 7th ed.; Cambridge University Press: Cambridge, UK, 1999.
118. Pawley, J.B. *Handbook of Biological Confocal Microscopy*; Springer: Berlin/Heidelberg, Germany, 2006.
119. Yuan, T.; Xu, Z.; Zhang, X.C. Development of terahertz wave microscopes. *Infrared Phys. Technol.* **2004**, *45*, 417–425. [[CrossRef](#)]
120. Blanchard, F.; Doi, A.; Tanaka, T.; Tanaka, K. Real-time, subwavelength terahertz imaging. *Annu. Rev. Mater. Res.* **2013**, *43*, 237–259. [[CrossRef](#)]
121. Hunsche, S.; Koch, M.; Brener, I.; Nuss, M.C. THz near-field imaging. *Opt. Commun.* **1998**, *150*, 22–26. [[CrossRef](#)]
122. Flammini, M.; Bonsi, C.; Ciano, C.; Giliberti, V.; Pontecorvo, E.; Italia, P.; DelRe, E.; Ortolani, M. Confocal terahertz imaging of ancient manuscripts. *J. Infrared Millim. Terahertz Waves* **2017**, *38*, 435–442. [[CrossRef](#)]
123. Salhi, M.A.; Pupeza, I.; Koch, M. Confocal THz laser microscope. *J. Infrared Millim. Terahertz Waves* **2010**, *31*, 358–366. [[CrossRef](#)]
124. Saeedkia, D. *Handbook of Terahertz Technology for Imaging, Sensing and Communications*; Volume in Woodhead Publishing Series in Electronics and Optical Materials; Saeedkia, D., Ed.; Elsevier: Amsterdam, The Nederland, 2013.
125. Adam, A.J.; Brok, J.M.; Seo, M.A.; Ahn, K.J.; Kim, D.S.; Kang, J.H.; Park, Q.H.; Nagel, M.; Planken, P.C. Advanced terahertz electric near-field measurements at sub-wavelength diameter metallic apertures. *Opt. Express* **2008**, *16*, 7407–7417. [[CrossRef](#)] [[PubMed](#)]
126. Mitrofanov, O.; Brener, I.; Harel, R.; Wynn, J.D.; Pfeiffer, L.N.; West, K.W.; Federici, J. Terahertz near-field microscopy based on a collection mode detector. *Appl. Phys. Lett.* **2000**, *77*, 3496. [[CrossRef](#)]
127. Iwami, K.; Ono, T.; Esashi, M. A New Approach to Terahertz Local Spectroscopy Using Microfabricated Scanning Near-Field Probe. *Jpn. J. Appl. Phys.* **2008**, *47*, 8095–8097. [[CrossRef](#)]
128. Cao, H.; Agrawal, A.; Nahata, A. Controlling the transmission resonance lineshape of a single subwavelength aperture. *Opt. Express* **2005**, *13*, 763–769. [[CrossRef](#)]
129. Keilmann, F.; Hillenbrand, R. Near-field microscopy by elastic light scattering from a tip. *Philos. Trans. Math. Phys. Eng. Sci.* **2004**, *362*, 787–805. [[CrossRef](#)]
130. Adam, A.J.L.; Brok, J.M.; Planken, P.C.M.; Seo, M.A.; Kim, D.S. THz near-field measurements of metal structure. *C. R. Phys.* **2008**, *9*, 161–168. [[CrossRef](#)]
131. Löffler, T.; Siebert, K.; Czasch, S.; Bauer, T.; Roskos, H.G. Visualization and classification in biomedical terahertz pulsed imaging. *Phys. Med. Biol.* **2002**, *47*, 3847–3852. [[CrossRef](#)]
132. Fitzgerald, A.J.; Wallace, V.P.; Pinder, S.E.; Purushotham, A.D.; O’Kelly, P.; Ashworth, P.C. Classification of terahertz-pulsed imaging data from excised breast tissue. *J. Biomed. Opt.* **2012**, *17*, 016005. [[CrossRef](#)]
133. Ushakov, A.; Chizhov, P.; Bukin, V.; Savel’ev, A.; Garnov, S. Broadband in-line terahertz 2D imaging: Comparative study with time-of-light, cross-correlation, and Fourier transform data processing. *J. Opt. Soc. Am. B* **2018**, *35*, 1159–1164. [[CrossRef](#)]
134. Wan, M.; Healy, J.J.; Sheridan, J.T. Terahertz phase imaging and biomedical applications. *Opt. Laser Technol.* **2020**, *122*, 105859. [[CrossRef](#)]
135. Dressel, M.; Grüner, G. *Electrodynamics of Solids*; Cambridge University Press: Cambridge, UK, 2002.
136. Kužel, P.; Němec, H.; Kadlec, F. Gouy shift correction for highly accurate refractive index retrieval in time-domain terahertz spectroscopy. *Opt. Express* **2010**, *18*, 15338–15348. [[CrossRef](#)] [[PubMed](#)]

137. Hegmann, F.A.; Ostroverkhova, O.; Cooke, D.G. Probing organic semiconductors with terahertz pulses. In *Photophysics of Molecular Materials*; Wiley: Hoboken, NJ, USA, 2000; pp. 367–428.
138. Llioyd-Hughes, J.; Jeon, T.I. A review of the terahertz conductivity of bulk and nano-materials. *J. Infrared Millim. Terahertz Waves* **2012**, *33*, 871–925. [[CrossRef](#)]
139. Guillet, J.P.; Recur, B.; Frederique, L.; Bousquet, B.; Canioni, L.; Manek-Hönniger, I.; Desbarats, P.; Mounaix, P. Review of Terahertz Tomography Techniques. *J. Infrared. Millim. Terahertz Waves* **2014**, *35*, 382–411. [[CrossRef](#)]
140. Mittleman, D.M. Twenty years of terahertz imaging. *Opt. Express* **2018**, *26*, 9417–9431. [[CrossRef](#)]
141. Ferguson, B.; Wang, S.; Gray, D.; Abbot, D.; Zhang, X.-C. T-ray computed tomography. *Opt. Lett.* **2002**, *27*, 1312–1314. [[CrossRef](#)]
142. Thrane, L.; Jacobsen, R.H.; Jepsen, P.U.; Keiding, S.R. THz reflection spectroscopy of liquid water. *Chem. Phys. Lett.* **1995**, *240*, 330–333. [[CrossRef](#)]
143. Cheon, H.; Yang, H.J.; Son, J.-H. Toward Clinical Cancer Imaging Using Terahertz Spectroscopy. *IEEE J. Sel. Top. Quantum Electron.* **2017**, *23*, 8600109. [[CrossRef](#)]
144. Zaytsev, K.I.; Gavdush, A.; Chernomyrdin, N.; Yurchenko, S. Highly accurate in vivo terahertz spectroscopy of healthy skin: Variation of refractive index and absorption coefficient along the human body. *IEEE Trans. Terahertz Sci. Technol.* **2015**, *5*, 817–827. [[CrossRef](#)]
145. Parrott, E.; Sy, S.; Blu, T.; Wallace, V.; Pickwell-MacPherson, E. Terahertz pulsed imaging in vivo: Measurements and processing methods. *J. Biomed. Opt.* **2011**, *16*, 106010. [[CrossRef](#)] [[PubMed](#)]
146. Kolesniko, A.; Kolesnikova, E.; Popov, A.; Nazarov, M.; Shkurinov, A.; Tuchin, V. In vitro terahertz monitoring of muscle tissue dehydration under the action of hyperosmotic agents. *Quantum Electron.* **2014**, *44*, 633. [[CrossRef](#)]
147. Smolyanskaya, O.; Schelkanova, I.; Kulya, M.; Odlyanitskiy, E.; Goryachev, I.; Tcypkin, A.; Grachev, Y.; Toropova, Y.; Tuchin, V. Glycerol dehydration of native and diabetic animal tissues studied by THz-TDS and NMR methods. *BOE* **2018**, *9*, 1198–1215. [[CrossRef](#)] [[PubMed](#)]
148. Fitzgerald, A.J.; Berry, E.; Zinov'ev, N.N.; Homer-Vanniasinkam, S.; Miles, R.E.; Chamberlain, J.M.; Smith, M.A. Catalogue of human tissue optical properties at terahertz frequencies. *J. Biol. Phys.* **2003**, *29*, 123–128. [[CrossRef](#)] [[PubMed](#)]
149. Kan, W.C.; Lee, W.S.; Cheung, W.H.; Wallace, V.P.; Pickwell-Macpherson, E. Terahertz pulsed imaging of knee cartilage. *BOE* **2010**, *1*, 967–974. [[CrossRef](#)] [[PubMed](#)]
150. Sun, Y.; Fischer, B.; Pickwell-MacPherson, E. Effects of formalin fixing on the terahertz properties of biological tissues. *J. Biomed. Opt.* **2009**, *14*, 064017. [[CrossRef](#)]
151. Fan, S.; Ung, B.; Parrott, E.P.J.; Pickwell-MacPherson, E. Gelatin embedding: A novel way to preserve biological samples for terahertz imaging and spectroscopy. *Phys. Med. Biol.* **2015**, *60*, 2703–2713. [[CrossRef](#)]
152. Gavdush, A.A.; Chernomyrdin, N.V.; Malakhov, K.M.; Beshplav, S.-I.T.; Dolganova, I.N.; Kosyrkova, A.V.; Nikitin, P.V.; Musina, G.R.; Katyba, G.M.; Reshetov, I.V.; et al. Terahertz spectroscopy of gelatin-embedded human brain gliomas of different grades: A road toward intraoperative THz diagnosis. *J. Biomed. Opt.* **2019**, *24*, 027001. [[CrossRef](#)]
153. Png, G.M.; Choi, J.W.; Ng, B.W.; Mickan, S.P.; Abbott, D.; Zhang, X.C. The impact of hydration changes in fresh bio-tissue on THz spectroscopic measurements. *Phys. Med. Biol.* **2008**, *53*, 3501. [[CrossRef](#)]
154. Sim, Y.; Park, J.; Ahn, K.-M.; Park, C.; Son, J.-H. Terahertz imaging of excised oral cancer at frozen temperature. *BOE* **2013**, *4*, 1413–1421. [[CrossRef](#)]
155. He, Y.; Ung, B.-Y.; Parrott, E.; Ahuja, A.; Pickwell-MacPherson, E. Freeze-thaw hysteresis effects in terahertz imaging of biomedical tissues. *BOE* **2016**, *7*, 4711–4717. [[CrossRef](#)] [[PubMed](#)]
156. Meng, K.; Chen, T.N.; Chen, T.; Zhu, T.G.; Liu, Q.; Li, Z.; Li, F.; Zhong, S.-C.; Li, Z.-R.; Feng, H.; et al. Terahertz pulsed spectroscopy of paraffin embedded brain glioma. *J. Biomed. Opt.* **2014**, *19*, 077001. [[CrossRef](#)] [[PubMed](#)]
157. Oh, S.J.; Kim, S.H.; Jeong, K.; Park, Y.; Huh, Y.M.; Son, J.H.; Suh, J.S. Measurement depth enhancement in terahertz imaging of biological tissues. *Opt. Express* **2013**, *21*, 21299–21305. [[CrossRef](#)] [[PubMed](#)]
158. Wang, Y.; Notake, T.; Tang, M.; Nawata, K.; Ito, H.; Minamide, H. Terahertz-wave water concentration and distribution measurement in thin biotissue based on a novel sample preparation. *Phys. Med. Biol.* **2011**, *56*, 4517. [[CrossRef](#)] [[PubMed](#)]
159. Wallace, V.P.; Fitzgerald, A.J.; Pickwell, E.; Pye, R.J.; Taday, P.F.; Flanagan, N.; Ha, T. Terahertz pulsed spectroscopy of human basal cell carcinoma. *Appl. Spectrosc.* **2006**, *60*, 1127–1133. [[CrossRef](#)] [[PubMed](#)]

160. Sun, Y.; Sy, M.Y.; Wang, Y.X.J.; Ahuja, A.T.; Zhang, Y.T.; Pickwell-MacPherson, E. A promising diagnostic method: Terahertz pulsed imaging and spectroscopy. *World J. Radiol.* **2011**, *3*, 55–65. [[CrossRef](#)]
161. Yeo, W.G.; Gurel, O.; Hitchcock, C.L.; Park, S.; Sertel, K.; Nahar, N.K. Evaluation of cancer tissue morphology via THz spectroscopic imaging: Human lung and small intestine malignancies. *Infrared Phys. Technol.* **2019**, *97*, 411–416. [[CrossRef](#)]
162. Wahaia, F.; Kasalyinas, I.; Minkevičius, L.; Carvalho Silva, C.D.; Urbanowicz, A.; Valušis, G. Terahertz spectroscopy and imaging for gastric cancer diagnosis. *J. Spectr. Imaging* **2020**, *9*, 1–8.
163. El-Shenawee, M.; Vohra, N.; Bowman, T.; Bailey, K. Cancer detection in excised breast tumors using terahertz imaging and spectroscopy. *Biomed. Spectrosc. Imaging* **2019**, *8*, 1–9. [[CrossRef](#)]
164. Cao, Y.; Huang, P.; Chen, J.; Ge, W.; Hou, D.; Zhang, G. Qualitative and quantitative detection of liver injury with terahertz time-domain spectroscopy. *BOE* **2020**, *11*, 982–993. [[CrossRef](#)]
165. Cao, Y.; Chen, J.; Huang, P.; Ge, W.; Hou, D.; Zhang, G. Inspecting human colon adenocarcinoma cell lines by using terahertz time-domain reflection spectroscopy. *Spectrochim. Acta* **2019**, *211*, 356–363. [[CrossRef](#)] [[PubMed](#)]
166. Kuzikova, A.V.; Grigorev, R.O.; Kurasova, A.P.; Demchenko, P.S.; Senyuk, A.V.; Zakharenko, A.A.; Belolipetskaya, J.R.; Khamid, A.H.; Khodzitsky, M.K. Study of refractive index of human stomach cancer tissue in THz frequency range. In Proceedings of the 6th International School and Conference “Saint Petersburg OPEN 2019”: Optoelectronics, Photonics, Engineering and Nanostructure, Saint Petersburg, Russia, 22–25 April 2019; Volume 1410, 012070.
167. Globus, T.; Moskaluk, C.; Pramoonjago, P.; Gelmont, B.; Moyer, A.; Bykhovski, A.; Ferrance, J. Sub-terahertz vibrational spectroscopy of ovarian cancer and normal control tissue for molecular diagnostic technology. *Cancer Biomark.* **2019**, *24*, 405–419. [[CrossRef](#)] [[PubMed](#)]
168. Yamaguchi, S.; Fukushi, Y.; Kubota, O.; Itsuji, T.; Ouchi, T.; Yamamoto, S. Origin and quantification of differences between normal and tumor tissues observed by terahertz spectroscopy. *Phys. Med. Biol.* **2016**, *68*, 6808–6820. [[CrossRef](#)] [[PubMed](#)]
169. Chau, D.Y.S.; Dennis, A.R.; Lin, H.; Zeitler, J.A.; Tunncliffe, A. Determination of Water Content in Dehydrated Mammalian Cells Using Terahertz Pulsed Imaging: A Feasibility Study. *Curr. Pharm. Biotechnol.* **2015**, *17*, 200–207. [[CrossRef](#)]
170. Smolyanskaya, O.A.; Chernomyrdin, N.V.; Konovko, A.A.; Zaytsev, K.I.; Ozheredov, I.A.; Cherkasova, O.P.; Nazarov, M.M.; Guillet, J.P.; Kozlov, S.A.; Kistenev, Y.V.; et al. Terahertz biophotonics as a tool for studies of dielectric and spectral properties of biological tissues and liquids. *Prog. Quantum Electron.* **2018**, *62*, 1–77. [[CrossRef](#)]
171. Brun, M.A.; Formanek, F.; Yasuda, A.; Sekine, M.; Ando, N.; Eishii, Y. Terahertz imaging applied to cancer diagnosis. *Phys. Med. Biol.* **2010**, *55*, 4615–4623. [[CrossRef](#)]
172. Chen, H.; Chen, T.H.; Tseng, T.F.; Lu, J.T.; Kuo, C.C.; Fu, S.C.; Lee, W.J.; Tsai, Y.F.; Huang, Y.Y.; Chuang, E.Y.; et al. High-sensitivity in vivo THz transmission imaging of early human breast cancer in a subcutaneous xenograft mouse model. *Opt. Express* **2011**, *19*, 21552–21562. [[CrossRef](#)]
173. Miura, Y.; Kamataki, A.; Uzuki, M.; Sasaki, T.; Nishizawa, J.I.; Sawai, T. Terahertz-wave spectroscopy for precise histopathological imaging of tumor and non-tumor lesions in paraffin sections. *J. Exp. Med.* **2011**, *223*, 291–296. [[CrossRef](#)]
174. Knobloch, P.; Schildknecht, C.; Kleine-Ostmann, T.; Koch, M.; Hoffmann, S.; Hofmann, M.; Rehberg, E.; Sperling, M.; Donhuijsen, K.; Hein, G.; et al. Medical THz imaging: An investigation of histo-pathological samples. *Phys. Med. Biol.* **2002**, *47*, 3875. [[CrossRef](#)]
175. Doradla, P.; Alavi, K.; Joseph, C.; Giles, R. Single-channel prototype terahertz endoscopic system. *J. Biomed. Opt.* **2014**, *19*, 080501. [[CrossRef](#)]
176. Reid, C.B.; Fitzgerald, A.; Reese, G.; Goldin, R.; Tekkis, P.; O’Kelly, P.S.; Pickwell-MacPherson, E.; Gibson, A.P.; Wallace, V.P. Terahertz pulsed imaging of freshly excised human colonic tissues. *Phys. Med. Biol.* **2011**, *56*, 4333–4353. [[CrossRef](#)] [[PubMed](#)]
177. Oh, S.J.; Kim, S.H.; Ji, Y.B.; Jeong, K.; Park, Y.; Yang, J.; Park, D.W.; Noh, S.K.; Kang, S.G.; Huh, Y.M.; et al. Study of freshly excised brain tissues using terahertz imaging. *BOE* **2014**, *5*, 2837–2842. [[CrossRef](#)] [[PubMed](#)]
178. Zhong, S. Progress in terahertz nondestructive testing: A review. *Front. Mech. Eng.* **2019**, *14*, 273–281. [[CrossRef](#)]

179. Bowman, T.C.; El-Shenawee, M.; Campbell, L.K. Terahertz Imaging of Excised Breast Tumor Tissue on Paraffin Sections. *IEEE Trans. Antennas Propag.* **2015**, *63*, 2088–2097. [[CrossRef](#)]
180. Danciu, M.; Alexa-Stratulat, T.; Stefanescu, C.; Dodi, G.; Tamba, B.I.; Mihai, C.T.; Stanciu, G.D.; Luca, A.; Spiridon, I.A.; Ungureanu, L.B.; et al. Terahertz Spectroscopy and Imaging: A Cutting-Edge Method for Diagnosing Digestive Cancers. *Materials* **2019**, *12*, 1519. [[CrossRef](#)] [[PubMed](#)]
181. Wallace, V.P.; MacPherson, E.; Fitzgerald, A.J.; Lo, T.; Provenzano, E.; Pinder, S.; Purushotham, A. Terahertz pulsed imaging and spectroscopy of breast tumors. In Proceedings of the Optical Methods in the Life Sciences, Boston, MA, USA, 1–3 October 2006.
182. Woodward, R.M.; Wallace, V.P.; Pye, R.J.; Cole, B.E.; Arnone, D.D.; Linfield, E.H.; Pepper, M. Terahertz pulse imaging of ex vivo basal cell carcinoma. *J. Invest. Dermatol.* **2003**, *120*, 72–78. [[CrossRef](#)]
183. Woodward, R.M.; Cole, B.E.; Wallace, V.P.; Pye, R.J.; Arnone, D.D.; Linfield, E.H.; Pepper, M. Terahertz pulse imaging in reflection geometry of human skin cancer and skin tissue. *Phys. Med. Biol.* **2002**, *47*, 3853. [[CrossRef](#)]
184. Wallace, V.P.; Fitzgerald, A.J.; Shankar, S.; Flanagan, N.; Pye, R.; Cluff, J.; Arnone, D.D. Dermatological Surgery and Lasers. Terahertz pulsed imaging of basal cell carcinoma ex vivo and in vivo. *Br. J. Dermatol.* **2004**, *151*, 424–432. [[CrossRef](#)]
185. Reese, G.; Reid, C.; Goldin, R.; Tran-Dang, M.A.; Fitzgerald, A.; Tekkis, P.; Wallace, V.P. Using terahertz pulsed imaging (TPI) to identify colonic pathology. In Proceedings of the 33rd International Conference on Infrared, Millimeter and Terahertz Waves, IEEE, Pasadena, CA, USA, 15–19 September 2008.
186. Wahaia, F.; Valusis, G.; Bernardo, L.M.; Almeida, A.; Moreira, J.A.; Lopes, P.C.; Macutkevicius, J.; Kasalynas, I.; Seliuta, D.; Adomavicius, R.; et al. Detection of colon cancer by terahertz techniques. *J. Mol. Struct.* **2011**, *1006*, 77–82. [[CrossRef](#)]
187. Fitzgerald, A.J.; Wallace, V.P.; Jimenez-Linan, M.; Bobrow, L.; Pye, R.J.; Purushotham, A.D.; Arnone, D.D. Terahertz pulsed imaging of human breast tumors. *Radiology* **2006**, *239*, 533–540. [[CrossRef](#)]
188. Bowman, T.C. *Experimental Terahertz Imaging and Spectroscopy for Ex-vivo Breast Cancer Tissue*; Master of Science in Electrical Engineering (Graduate), University of Arkansas: Fayetteville, AR, USA, August 2014.
189. Ashworth, P.C.; Pickwell-MacPherson, E.; Provenzano, E.; Pinder, S.E.; Purushotham, A.D.; Pepper, M.; Wallace, V.P. Terahertz pulsed spectroscopy of freshly excised human breast cancer. *Opt. Express* **2009**, *17*, 12444–12454. [[CrossRef](#)] [[PubMed](#)]
190. Bowman, T.; Wu, Y.; Gauch, J.; Campbell, L.K.; El-Shenawee, M. Terahertz Imaging of Three-Dimensional Dehydrated Breast Cancer Tumors. *J. Infrared Millim. Terahertz Waves* **2017**, *38*, 766–786. [[CrossRef](#)]
191. Eadie, L.H.; Reid, C.B.; Fitzgerald, A.J.; Wallace, V.P. Optimizing multi-dimensional terahertz imaging analysis for colon cancer diagnosis. *Expert Syst. Appl.* **2013**, *40*, 2043–2205. [[CrossRef](#)]
192. Santaolalla, A.; Sheikh, M.; Van Hemelrijck, M.; Portieri, A.; Coolen, A.C.C. Improved resection margins in breast-conserving surgery using Terahertz Pulsed imaging data. *arXiv* **2018**, arXiv:1805.01349.
193. Zaytsev, K.I.; Chernomyrdin, N.V.; Kudrin, K.C.; Gavdush, A.A.; Nosova, P.A.; Yurchenko, S.O.; Reshetov, I.V. In vivo terahertz pulsed spectroscopy of dysplastic and non-dysplastic skin nevi. *J. Phys. Conf. Ser.* **2016**, *735*, 012076. [[CrossRef](#)]
194. Zaytsev, K.I.; Kudrin, K.G.; Karasik, V.E.; Reshetov, I.V.; Yurchenko, S.O. In vivo terahertz spectroscopy of pigmented skin nevi: Pilot study of non-invasive early diagnosis of dysplasia. *Appl. Phys. Lett.* **2015**, *106*, 053702. [[CrossRef](#)]
195. Grootendorst, M.R.; Fitzgerald, A.J.; Brouwer, S.G.; de Koning, S.A.; Portieri, A.; Van Hemelrijck, M.; Young, M.R.; Owen, J.; Cariati, M.; Pepper, M.; et al. Use of a handheld terahertz pulsed imaging device to differentiate benign and malignant breast tissue. *BOE* **2017**, *8*, 2932–2945. [[CrossRef](#)]
196. Matsuura, Y.; Takeda, E. Hollow optical fibers loaded with an inner dielectric film for terahertz broadband spectroscopy. *JOSA* **2008**, *25*, 1949–1954. [[CrossRef](#)]
197. Doradla, P.; Joseph, C.S.; Kumar, J.; Giles, R.H. Characterization of bending loss in hollow flexible terahertz waveguides. *Opt. Express* **2012**, *20*, 19176–19184. [[CrossRef](#)]
198. Doradla, P.; Joseph, C.S.; Kumar, J.; Giles, R.H. Propagation loss optimization in metal/dielectric coated hollow flexible terahertz waveguides. *Proc. SPIE* **2012**, *8261*, 82610P1–82610P10.

199. Ji, Y.B.; Lee, E.S.; Kim, S.-H.; Son, J.H.; Jeon, T.I. A miniaturized fiber-coupled terahertz endoscope system. *Opt. Express* **2009**, *17*, 17082–17087. [[CrossRef](#)] [[PubMed](#)]
200. Gonzalez, R.C.; Woods, R.E. *Digital Image Processing*, 3rd ed.; Pearson Prentice Hall: Upper Saddle River, NJ, USA, 2008; pp. 120–144.
201. Pratt, W.K. *Digital Image Processing*, 4th ed.; John Wiley & Sons: Hoboken, NJ, USA, 2007; pp. 288–291.
202. Canny, J.F. A Computational Approach to Edge Detection. *IEEE Trans. Pattern Anal. Mach. Intell.* **1986**, *8*, 679–698. [[CrossRef](#)] [[PubMed](#)]
203. Ji, Y.B.; Moon, I.-S.; Bark, H.S.; Kim, S.H.; Park, D.W.; Noh, S.K.; Huh, Y.-M.; Suh, J.-S.; Oh, S.J.; Jeon, T.-I. Terahertz otoscope and potential for diagnosis otitis media. *BOE* **2016**, *7*, 1201. [[PubMed](#)]
204. Hernandez-Cardoso, G.G.; Rojas-Landeros, S.C.; Alfaro-Gomez, M.; Hernandez-Serrano, A.I.; Salas-Gutierrez, I.; Lemus-Bedolla, E.; Castillo-Guzman, A.R.; Lopez-Lemus, H.L.; Castro-Camus, E. Terahertz imaging for early screening of diabetic foot syndrome: A proof of concept. *Sci. Rep.* **2017**, *7*, 42124. [[CrossRef](#)] [[PubMed](#)]
205. Jung, E.; Lim, M.H.; Moon, K.W.; Do, Y.W.; Lee, S.S.; Han, H.W.; Choi, H.J.; Cho, K.S.; Kim, K.R. Terahertz pulse imaging of micro-metastatic lymph nodes in early-stage cervical cancer patients. *J. Opt. Soc.* **2011**, *15*, 155–160. [[CrossRef](#)]
206. Ji, Y.B.; Oh, S.J.; Kang, S.G.; Heo, J.; Kim, S.H.; Choi, Y.; Song, S.; Son, S.H.; Lee, J.H.; Haam, S.J.; et al. Terahertz reflectometry imaging for low and high grade gliomas. *Sci. Rep.* **2016**, *6*, 36040. [[CrossRef](#)]
207. Kashanian, H.A.; Ghaary, H.B.; Bagherzadeh, N.C. Gastric Cancer Diagnosis Using Terahertz Imaging. *Majlesi J. Multimed. Process.* **2015**, *4*, 1–7.
208. Ji, Y.B.; Kim, S.-H.; Jeong, K.; Choi, Y.; Son, J.-H.; Park, D.W.; Noh, S.K.; Jeon, T.-I.; Huh, Y.-M.; Seungjoo, H.; et al. Terahertz spectroscopic imaging and properties of gastrointestinal tract in a rat model. *BOE* **2014**, *5*, 4162–4170. [[CrossRef](#)]
209. Ji, Y.B.; Park, C.H.; Kim, H.; Kim, S.H.; Lee, G.M.; Noh, S.K.; Jeon, T.-I.; Son, J.-H.; Huh, Y.-M.; Seungjoo, H.; et al. Feasibility of terahertz reflectometry for discrimination of human early gastric cancers. *BOE* **2015**, *6*, 1398–1406. [[CrossRef](#)]
210. Sim, Y.C.; Ahn, K.-M.; Park, J.Y.; Park, C.; Son, J.-H. Temperature-Dependent Terahertz Imaging of Excised Oral Malignant Melanoma. *IEEE J. Biomed. Health Inform.* **2013**, *17*, 779. [[CrossRef](#)]
211. Taylor, Z.D.; Singh, R.S.; Bennett, D.B.; Tewari, P.; Kealey, C.P.; Bajwa, N.; Culjat, M.O.; Hubschman, J.; Brown, E.R.; Grundfest, W.S. THz Medical Imaging: In vivo Hydration Sensing. *IEEE Trans. Terahertz Sci. Technol.* **2011**, *1*, 201–219. [[CrossRef](#)]
212. Wilmink, G.J.; Grundt, J.E. Current State of Research on Biological Effects of Terahertz Radiation. *J. Infrared Millim. Terahertz Waves* **2011**, *32*, 1074–1122. [[CrossRef](#)]
213. Humphreys, K.; Loughran, J.P.; Gradziel, M.; Lanigan, W.; Ward, T.; Murphy, J.A.; O’Sullivan, C. Medical applications of terahertz imaging: A review of current technology and potential applications in biomedical engineering. In Proceedings of the 26th Annual International Conference of the IEEE Engineering in Medicine and Biology Society, San Francisco, CA, USA, 1–5 September 2004.
214. Arnone, D.D.; Ciesla, C.M.; Corchia, A.; Egusa, S.; Pepper, M.; Chamberlain, J.M.; Bezant, C.; Linfield, E.H.; Clothier, R.; Khammo, N. Applications of terahertz (THz) technology to medical imaging. In Proceedings of the Terahertz Spectroscopy and Applications II, Munich, Germany, 16–18 June 1999; Volume 3828.
215. Zinov’ev, N.N.; Fitzgerald, A.F.; Strafford, S.M.; Wood, D.J.; Carmichael, F.A.; Miles, R.E.; Smith, M.A.; Chamberlain, J.M. Identification of tooth decay using terahertz imaging and spectroscopy. In Proceedings of the Twenty Seventh International Conference on Infrared and Millimeter Waves, San Diego, CA, USA, 22–26 September 2002.
216. Crawley, D.A.; Longbottom, C.; Cole, B.E.; Ciesla, C.M.; Arnone, D.; Wallace, V.P.; Pepper, M. Terahertz pulse imaging: A pilot study of potential applications in dentistry. *Caries Res.* **2003**, *37*, 352–359. [[CrossRef](#)]
217. Crawley, D.; Longbottom, C.; Wallace, V.P.; Cole, B.; Arnone, D.; Pepper, M. Three-dimensional terahertz pulse imaging of dental tissue. *J. Biomed. Opt.* **2003**, *8*, 303–307. [[CrossRef](#)]
218. Kamburoğlu, K.; Karagöz, B.; Altan, H.; Özen, D. An ex vivo comparative study of occlusal and proximal caries using terahertz and X-ray imaging. *Dentomaxillofac. Radiol.* **2019**, *48*, 20180250. [[CrossRef](#)]

219. Kamburoğlu, K.; Kurt, H.; Kolsuz, E.; Öztaş, B.; Tatar, I.; Çelik, H.H. Occlusal caries depth measurements obtained by five different imaging modalities. *J. Digit. Imaging* **2011**, *24*, 804–813. [[CrossRef](#)]
220. Torres, M.G.; Santos, A.S.; Neves, F.S.; Arriaga, M.L.; Campos, P.S.F.; Crusoé-Rebello, I. Assessment of enamel-dentin caries lesions detection using bitewing PSP digital images. *J. Appl. Oral Sci.* **2011**, *19*, 462–468. [[CrossRef](#)]



© 2020 by the authors. Licensee MDPI, Basel, Switzerland. This article is an open access article distributed under the terms and conditions of the Creative Commons Attribution (CC BY) license (<http://creativecommons.org/licenses/by/4.0/>).